nature biotechnology

Article

https://doi.org/10.1038/s41587-024-02339-4

A CAR enhancer increases the activity and persistence of CAR T cells

Received: 14 July 2023

Accepted: 27 June 2024

Published online: 30 July 2024

Check for updates

Taha Rakhshandehroo[1], Shreya R. Mantri[1,7], Heydar Moravej[1,7], Benjamin B. V. Louis[1,7], Ali Salehi Farid[1], Leila Munaretto[1], Kathryn Regan[2], Radia M. M. Khan[1], Alexandra Wolff[1], Zoe Farkash[1], Min Cong[1], Adrien Kuhnast[1], Ali Nili[1], Uk-Jae Lee[1], Harris H. Allen[1], Lea Berland[1], Ester Simkova[1], Safak C. Uslu[1], Soheil Tavakolpour[1], Jennifer E. Rowley[1,2], Elisabeth Codet[1], Haneyeh Shahbazian[1], Jessika Baral[1,3], Jason Pyrdol[1], Caron A. Jacobson[3,4], Omar Nadeem[3,4], Hadi T. Nia[2], Kai W. Wucherpfennig[1,3,5] & Mohammad Rashidian[1,3,5,6]

Although chimeric antigen receptor (CAR) T cell therapies have demonstrated promising clinical outcomes, durable remissions remain limited. To extend the efficacy of CAR T cells, we develop a CAR enhancer (CAR-E), comprising a CAR T cell antigen fused to an immunomodulatory molecule. Here we demonstrate this strategy using B cell maturation antigen (BCMA) CAR T cells for the treatment of multiple myeloma, with a CAR-E consisting of the BCMA fused to a low-affinity interleukin 2 (IL-2). This selectively induces IL-2 signaling in CAR T cells upon antigen–CAR binding, enhancing T cell activation and antitumor activity while reducing IL-2-associated toxicities. We show that the BCMA CAR-E selectively binds CAR T cells and increases CAR T cell proliferation, clearance of tumor cells and development of memory CAR T cells. The memory cells retain the ability to re-expand upon restimulation, effectively controlling tumor growth upon rechallenge. Mechanistic studies reveal the involvement of both CAR and IL-2 receptor endodomains in the CAR-E mechanism of action. The CAR-E approach avoids the need for specific engineering and enables CAR T cell therapy with lower cell doses.

Chimeric antigen receptor (CAR) T cell therapy is being extensively investigated as a standalone treatment or in combination with other therapies for various solid tumors, hematological malignancies and autoimmune disorders[1–5]. Six CAR T cell therapies have received Food and Drug Administration approval[6], including four that target cluster of differentiation 19 (CD19) in B cell leukemias and lymphomas and two that target B cell maturation antigen (BCMA) in multiple myeloma (MM). BCMA is preferentially expressed in mature B lymphocytes and shows minimal expression in hematopoietic stem cells or nonhematopoietic tissue. It has a crucial role in the survival of bone marrow plasma cells without notably impacting overall B cell homeostasis and is an important marker on malignant plasma cells in MM. BCMA CAR T cells have demonstrated remarkable efficacy in heavily pretreated persons with MM, with studies reporting an overall response rate of 80%, even in persons with extramedullary lesions[2,3,7]. Despite this progress, critical challenges remain, particularly in terms of the

[1]Department of Cancer Immunology and Virology, Dana-Farber Cancer Institute, Boston, MA, USA. [2]Department of Biomedical Engineering, Boston University, Boston, MA, USA. [3]Harvard Medical School, Boston, MA, USA. [4]Department of Medical Oncology, Dana-Farber Cancer Institute, Boston, MA, USA. [5]Parker Institute for Cancer Immunotherapy, San Francisco, CA, USA. [6]Department of Radiology, Brigham and Women's Hospital, Harvard Medical School, Boston, MA, USA. [7]These authors contributed equally: Shreya R. Mantri, Heydar Moravej, Benjamin B. V. Louis. e-mail: Mohammad_rashidian@dfci.harvard.edu

duration of response. For instance, half of the persons treated with the CAR T therapy idecabtagene vicleucel experience disease relapse within 1 year, coinciding with the disappearance of CAR T cells from the bloodstream[2,3,8]. Notably, the majority of relapses remain BCMA positive[8,9]. For example, in idecabtagene vicleucel-treated participants, BCMA-expressing bone marrow tumor cells were observed in all six biopsy samples taken at disease progression. Soluble BCMA was detectable in 82 of 84 evaluable participants at disease progression[8]. This suggests that antigen loss is not the major mechanism behind relapse. Although more promising results were observed with the CAR T cell therapy ciltacabtagene autoleucel, long-term data are needed to gain a comprehensive understanding of its relapse rate[10].

Several strategies have been developed to enhance CAR T cell activity and persistence, including (1) the choice of costimulatory domain such as 4-1BB, CD28 or their combinations[11–15]; (2) the use of genome-editing technologies to regulate exhaustion or activation pathways[16–20]; (3) the use of inducible systems to equip CAR T cells with the capacity to express cytokines and their receptors such as interleukin-7 (IL-7), IL-12, IL-15 or their combinations[21–25]; and (4) the use of switch constructs that feature a receptor designed to bind to an inhibitory molecule (for example, IL-4), while the intracellular domain is engineered to induce T cell fitness (for example, IL-7 endodomain)[26,27]. An interesting approach used an orthogonal IL-2 and IL-2 receptor (IL-2R) system to preferentially deliver the orthogonal IL-2 to the ortho-IL-2R-engineered CAR T cells[28]. Alternative methods have been devised to facilitate interactions between CAR T cells and dendritic cells, thereby providing costimulation through dendritic cells[29,30]. These multifaceted strategies hold great promise but necessitate additional engineering steps on CAR T cells, resulting in inherent challenges such as intricate design and operation, potential immunogenicity and the risk of potential DNA mutations. Additionally, further genetic modification of CAR T cells may worsen toxicity. Consequently, despite considerable effort, these approaches have had limited clinical application. To overcome these limitations without introducing additional genetic modifications to CAR T cells, we developed antigen-based CAR enhancers (CAR-Es). This method involves fusing a target antigen (for example, BCMA) with a low-affinity enhancer molecule (for example, IL-2), allowing for precise targeting of CAR T cells and facilitating the preferential delivery of immune-modulating agents after infusion. As the enhancer molecule, we chose to use the IL-2 cytokine, which promotes the activation of T cells and enhances their antitumor activity. Our findings demonstrate that the CAR-E selectively enhances the functionality and persistence of CAR T cells. This approach offers an off-the-shelf treatment option, allowing for the optimization of dosage and treatment schedules to minimize potential toxicity.

Results

Design and development of the BCMA CAR-E

We constructed a fusion protein consisting of the human BCMA protein ectodomain fused with a low-affinity mutant human IL-2 dimer (referred to as 'mutIL-2')[31]. The mutIL-2 molecule contains two substitutions (H16A and F42A) that decrease its affinity for human IL-2Rβ (3-fold; K_D of ~610 nM) and IL-2Rα (CD25) (110-fold; K_D of ~1,200 nM)[31] (Fig. 1a). Consequently, the BCMA–mutIL-2 fusion protein preferentially delivers the low-affinity IL-2 molecule to the surface of CAR T cells through antigen-to-CAR-specific binding, minimizing effects on normal T cells, regulatory T cells or systemic toxicity.

To improve pharmacokinetics and enhance stability, we incorporated the CH3 domain of human immunoglobulin G1 (IgG1) (approximately 14 kDa in size) between the antigen and the mutIL-2 molecule (Fig. 1a). To facilitate purification through Ni-NTA affinity chromatography and for in vitro characterization and in vivo assessment of the pharmacokinetic properties of the fusion protein, a C-terminal 6xHis-tag and a FLAG tag (DYKDDDDK) were included in the design. The BCMA–mutIL-2 protein was expressed in HEK293T cells and purified using standard methods at a yield of approximately 40 mg l^{-1}. The purity of the protein was validated by SDS–PAGE analyses (Supplementary Fig. 1).

In vitro characterization of the BCMA CAR-E

To assess the binding affinity of BCMA–CH3–mutIL-2 (referred to as 'BCMA CAR-E'), flow cytometric analysis was performed by staining BCMA CAR T cells with varying concentrations of the BCMA CAR-E. We observed a half-maximal effective concentration (EC_{50}) of ~0.21 nM for the BCMA CAR-E. Minimal binding of the CAR-E to nontransduced T cells was noted, along with minimal binding of VHH–mutIL-2, a control construct that replaced the BCMA ectodomain with an irrelevant nanobody (VHH) in the CAR-E, to BCMA CAR T cells (Fig. 1b). This provides additional evidence that the binding of the CAR-E to CAR T cells is primarily driven by the BCMA and that the mutIL-2 molecule exhibits weak binding to both CAR T and nontransduced T cells. The BCMA–mutIL-2 CAR-E did not exhibit binding to any immune cell populations in human peripheral blood mononuclear cells (PBMCs) (Supplementary Fig. 2).

Next, we evaluated the functional effects of the BCMA CAR-E on BCMA CAR T cells. After a 24-h resting period without cytokines, CAR T cells were incubated with varying concentrations of the BCMA–mutIL-2 CAR-E for 24 h, followed by an assessment of the expression of the CD69 activation marker[32] using flow cytometric analysis. The results demonstrated a dose-dependent and selective increase in CD69 expression on CAR T cells (Fig. 1c), while no effect was observed on nontransduced T cells (Fig. 1d). Moreover, the BCMA CAR-E treatment resulted in a significantly higher increase in CD69 expression compared to VHH–mutIL-2, BCMA–CH3 or their combination, suggesting that the observed effect is only evident when the low-affinity IL-2 molecule is fused to the antigen.

The BCMA CAR-E does not inhibit killing efficacy of CAR T cells

To test whether the BCMA CAR-E inhibits the killing activity of BCMA CAR T cells, a killing assay was conducted using CAR T cells and patient-derived $BCMA^+$ OPM2 cancer cells in the presence of varying concentrations of the BCMA CAR-E. The results demonstrated no inhibition of killing even at the highest tested concentration (100 nM) of the CAR-E (Fig. 1e). Incubating the CAR-E treatment for 3 h and subsequently removing it, mimicking in vivo conditions, or maintaining the BCMA CAR-E throughout the entire 40-h killing assay did not markedly affect the killing efficacy of CAR T cells. Of note, as anticipated, the addition of the control VHH–mutIL-2 molecule did not affect killing efficacy either (Fig. 1e).

The CAR-E selectively induces signal transducer and activator of transcription 5 (STAT5) activity in CAR T cells

To evaluate the impact of the BCMA CAR-E on STAT5 activity, BCMA CAR T cells were exposed to varying concentrations of the CAR-E. Following a 5-min incubation at 37 °C, cells were fixed and stained for pY694 STAT5. The results revealed that the BCMA–mutIL-2 CAR-E induced phosphorylation of STAT5 in CAR T cells with an EC_{50} of ~0.014 nM (Fig. 1f). In contrast, the VHH–mutIL-2 molecule required a higher concentration (EC_{50} = 3.9 nM) to induce STAT5 phosphorylation, indicating an over 200-fold decrease in sensitivity. Wild-type IL-2 exhibited a lower EC_{50} (approximately 0.001 nM). BCMA CAR T cells preblocked with BCMA–CH3 showed a significant decrease in phosphorylated STAT5 (pSTAT5) levels to the same degree as control VHH–mutIL-2, validating that the potency of the CAR-E is mediated through antigen-to-CAR binding (Fig. 1f). To determine whether the CAR-E binding to a target cell can result in STAT5 signaling in an adjacent cell (*trans*-activation), nonblocked and preblocked BCMA CAR T cells were cocultured in the presence of varying concentrations of the CAR-E. Preblocked CAR T cells illustrated lower pSTAT5 levels compared to their cocultured

https://doi.org/10.1038/s41587-024-02339-4

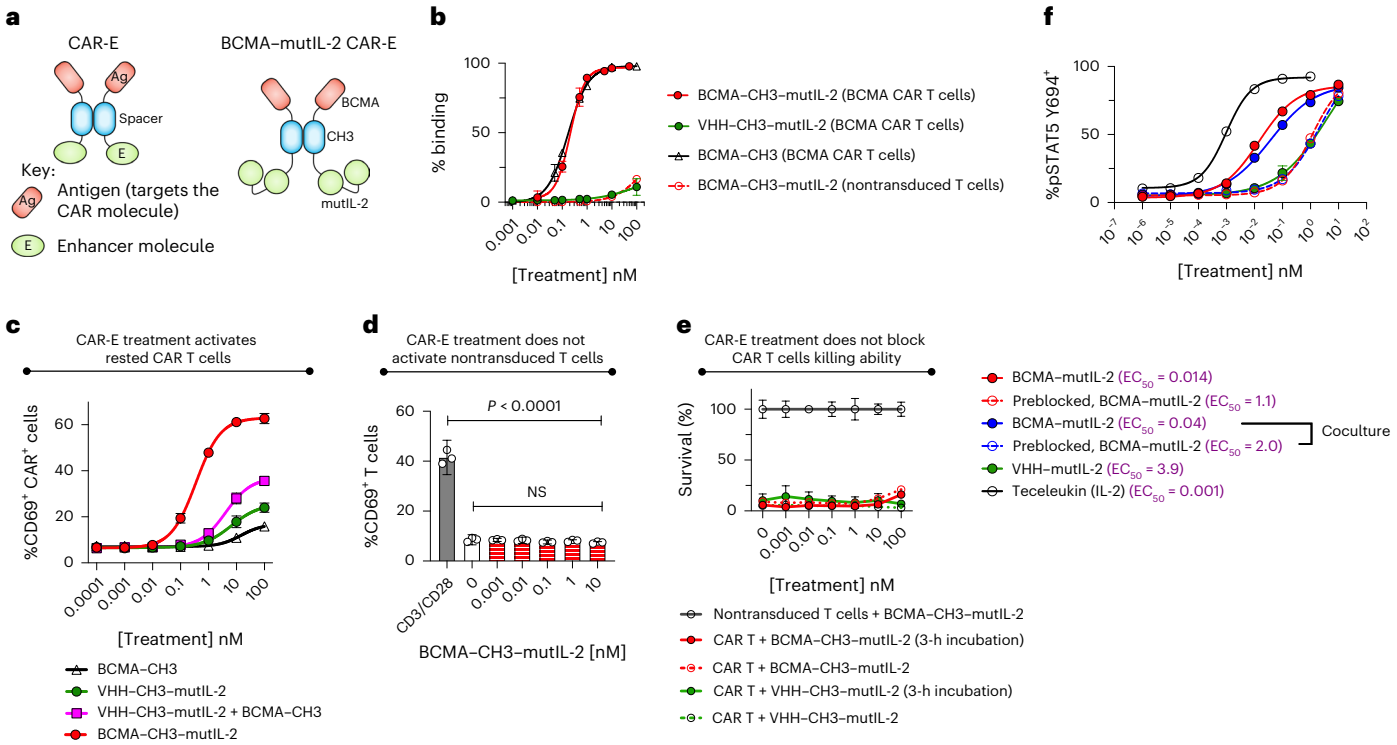

Fig. 1 | Design and characterization of the BCMA CAR-E. a, Schematic of the CAR-E therapeutic platform. Left: the general design of the CAR-E. Right: the structure of the developed BCMA–mutIL-2 CAR-E. **b**, The BCMA–mutIL-2 CAR-E binds to BCMA CAR T cells with high specificity and affinity. Nontransduced T cells and VHH–mutIL-2 were used as controls. A secondary AlexaFluor647-labeled anti-FLAG antibody was used for staining. Error bars represent the mean ± 95% CI. **c**,**d**, Incubation of rested BCMA CAR T cells for 24 h with the BCMA CAR-E treatment results in dose-dependent activation of CAR T cells (**c**) but not nontransduced T cells (**d**). In **c**, the results of the unpaired *t*-test indicated a statistically significant ($P \leq 0.0001$) increase in activation in the BCMA–mutIL-2 treatment group compared to the VHH–mutIL-2, BCMA–CH3 or their combination control groups at a concentration of 0.1 nM or higher. Error bars represent the mean ± 95% CI. In **d**, no treatment and CD3–CD28 activation were used as negative and positive controls, respectively. Error bars represent the mean ± 95% CI. An unpaired two-sided *t*-test was used. NS, not significant. **e**, The BCMA–mutIL-2 CAR-E does not block the killing efficacy of the CAR T cells. OPM2 cells were coincubated with BCMA CAR T cells or nontransduced T cells (E:T ratio of 1:1; 30,000 cells of each) in the presence of varying concentrations of the CAR-E or the control VHH–mutIL-2. Treatments were allowed to remain in the mixture either for the entire duration of the experiment or for 3 h, as indicated in the legend. Live (PI^-) OPM2 cells were counted 40 h later. Error bars represent the mean ± s.d. **f**, The BCMA–mutIL-2 CAR-E results in the phosphorylation of STAT5 in CAR T cells. The percentage of CAR T cells stained positive for pSTAT5 is shown, as assessed by flow cytometry. BCMA CAR T cells were treated with the indicated treatments followed by the assessment of STAT5 phosphorylation. For the preblocking experiments, the BCMA CAR T cells were treated with BCMA–CH3 (100 nM) for 20 min at 4 °C before exposure to the CAR-E treatment at 37 °C. Error bars represent the mean ± s.d. For **b**–**f**, $n = 3$ technical replicates for each point.

nonblocked CAR T cells, indicating that the CAR-E affects the targeted CAR T cells (*cis*-activation) and not any adjacent cells.

Taken together, the analysis of STAT5 activity supports the notion that the BCMA CAR-E exerts its influence on targeted CAR T cells through the *cis* delivery of the low-affinity IL-2, with the effect mediated by antigen-to-CAR binding.

The CAR-E slowly internalizes at 37 °C

Considering that T cells rapidly internalize IL-2R within minutes of IL-2 binding[33], we assessed the internalization of the CAR-E using the fluorescently labeled BCMA–mutIL-2 CAR-E. In short, BCMA CAR T cells were exposed to AlexaFluor647-labeled BCMA–mutIL-2, BCMA–CH3 or VHH–mutIL-2 at a concentration of 2 nM. The cells were incubated at either 4 °C or 37 °C for various time intervals, followed by fixation and subsequent microscopy imaging. We observed that, as anticipated, the control VHH–mutIL-2 underwent rapid internalization within 30 min at 37 °C, whereas the internalization of the BCMA–mutIL-2 CAR-E was significantly slower (Supplementary Fig. 3). Notably, the internalization rate of BCMA–CH3 was slower than that of the BCMA–mutIL-2 CAR-E, suggesting that the low-affinity IL-2 likely contributes to the internalization rate of the CAR-E compared to BCMA–CH3 molecules. The experiment was repeated with similar settings and yielded consistent results (Supplementary Fig. 4).

These findings suggest that the BCMA CAR-E prolongs the interaction between the low-affinity IL-2 molecules and the IL-2R, potentially leading to a prolonged IL-2 signaling response.

The CAR-E enhances persistence of CAR T cells in an MM model

Pharmacokinetic studies illustrated that, as anticipated, the circulatory half-life of the CAR-E was short (1–1.5 h) (Fig. 2a). To assess the impact of the CAR-E treatment on CAR T cell persistence in vivo, we used an MM xenograft mouse model using OPM2 engrafted in immunocompromised NOD-*scid* IL-2rγ^{null} (NSG) mice. NSG mice were intravenously injected with OPM2 cells (1 million), followed by BCMA CAR T cells 2 weeks later (0.5 million CAR^+ cells; 4-1BB–CD3ζ CAR construct), with a subset also receiving the BCMA–mutIL-2 CAR-E treatment (Fig. 2b). After 1 month or longer, mice were euthanized and flow cytometric analyses were performed on the isolated organs. Our findings revealed a significant presence of CAR T cells in the spleen and bone marrow of the BCMA–mutIL-2 CAR-E-treated group compared to nontreated animals (Fig. 2c). These experiments were replicated multiple times with similar outcomes (Fig. 2d, Supplementary Fig. 5 and Supplementary Table 1). An additional control group receiving CAR T cells plus VHH–mutIL-2 treatment ($n = 7$) did not exhibit significant expansion or persistence of CAR T cells compared to the control group receiving only CAR T cells without treatment (Fig. 2d). These results suggest that

https://doi.org/10.1038/s41587-024-02339-4

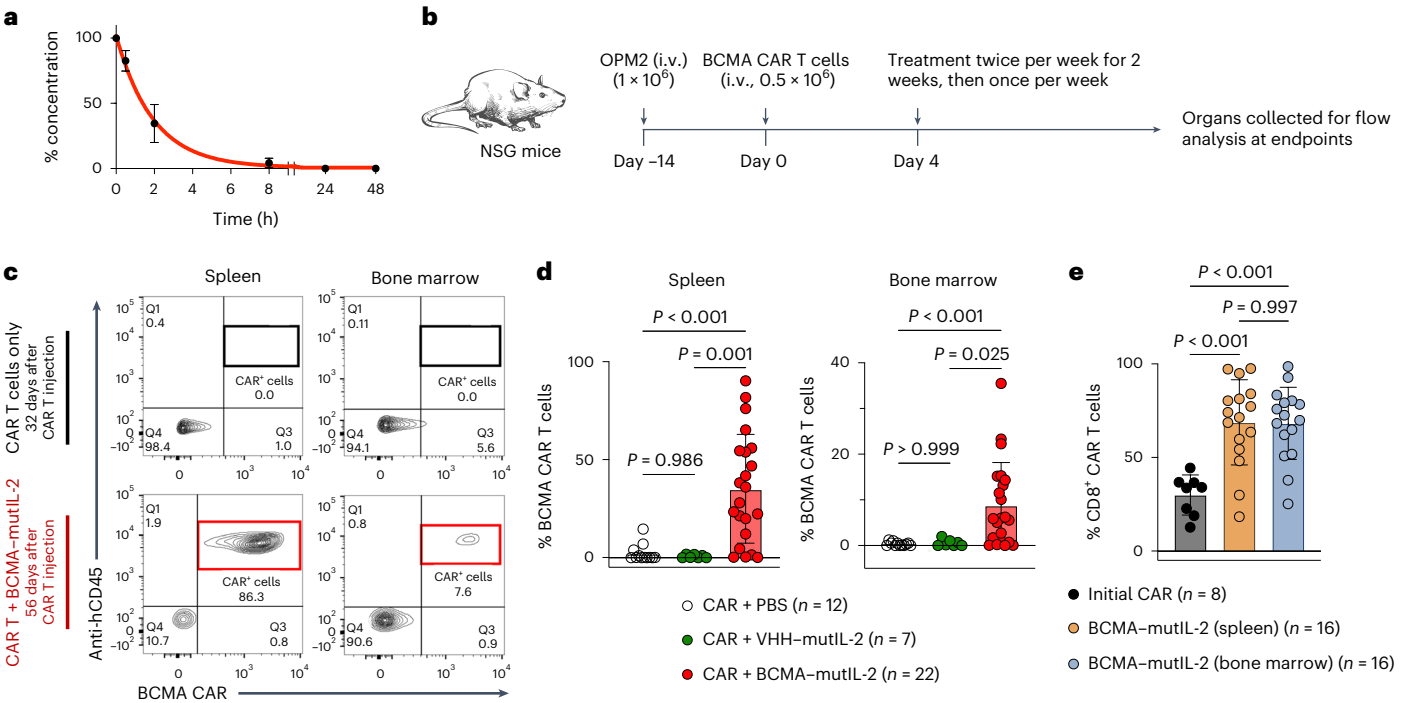

Fig. 2 | CAR-E treatment results in enhanced persistence of CAR T cells in vivo. a, Assessment of the circulating half-life of the BCMA CAR-E. NSG mice were administered 8 mg kg^{-1} of the BCMA–mutIL-2 CAR-E (i.p., $n = 3$). Blood samples were collected by tail-vein puncture at five different time points (30 min, 2 h, 8 h, 24 h and 48 h) after administration. An ELISA was performed to determine the concentration of the treatments in the sera. The circulating half-life was estimated to be ~1.5 h. Error bars represent the mean ± s.d. **b**, NSG mice were injected with OPM2 (human MM) cells followed by BCMA CAR (human) T cell administration according to the schedule. The BCMA–mutIL-2 CAR-E treatment (200 µg or less per dose, as indicated in Supplementary Fig. 5) was administered twice per week for 2 weeks, followed by once per week until the endpoint. **c**, Flow cytometric analyses performed 1 month or longer after injection of CAR T cells showed persistence of BCMA CAR T cells in the spleen (left) and bone marrow (right) of treated mice compared to control mice. BCMA CAR T cells were detected by costaining with an anti-human CD45 antibody and AlexaFluor647-labeled BCMA. Similar results were obtained in repeated experiments. Additional control cohorts received VHH–mutIL-2 treatment with the same dose and schedule (200 µg or less per dose, as indicated in Supplementary Fig. 5). **d**, Pooled data from the experiments in **c** are shown. PBMCs from four different donors were used for the experiments. A one-way analysis of variance (ANOVA) with a post hoc Tukey's test was used for normal data (spleen) and a Kruskal–Wallis test with a post hoc Dunn's test was used for non-normal data (bone marrow). Individual flow graphs for the pooled data are presented in Supplementary Fig. 5 and summarized in Supplementary Table 1. Error bars represent the mean ± s.d. **e**, Further analyses revealed that BCMA–mutIL-2 treatment had a stronger effect on CD8$^+$ CAR T cells, increasing their proportion from ~30% to ~70% of total CD4$^+$ and CD8$^+$ CAR T cells. 'CAR + VHH–mutIL-2' or 'CAR + PBS' cohorts did not yield sufficient persisting CAR T cells for similar analyses. Data were analyzed by group mean comparisons using a one-way ANOVA and subsequent Tukey post hoc analysis. Error bars represent the mean ± s.d.

the BCMA–mutIL-2 CAR-E can lead to enhanced persistence of CAR T cells in vivo and that the BCMA component in the CAR-E is essential for its effect on CAR T cells, consistent with the in vitro findings. Further analysis revealed that the BCMA–mutIL-2 treatment had a more pronounced effect on CD8$^+$ CAR T cells, resulting in a significant increase in their proportion (Fig. 2e). The cohorts receiving only CAR T cells or CAR T cells with VHH–mutIL-2 control treatment did not yield a sufficient number of persistent CAR T cells for comparable analysis.

Furthermore, flow cytometric analyses of the spleen and bone marrow, gating on green fluorescent protein (GFP)-positive OPM2 cells at the endpoint, revealed that several animals had completely eliminated tumor cells, regardless of the treatment. Specifically, 6 of 12 mice from the 'CAR T cell + PBS' cohort, 4 of 7 from the 'CAR T cell + VHH–mutIL-2' cohort and all 22 mice from the 'CAR T cell + CAR-E' cohort fully cleared the tumor cells from their spleen, bone marrow and liver (Supplementary Fig. 5 and Supplementary Table 1). This outcome is likely attributable to the clinically relevant dose of CAR T cells used in this experiment. It is noteworthy that potential relapses at longer time points may occur; however, not all mice were monitored for potential relapse in this experiment as the main objective was to investigate the persistence of CAR T cells. Nevertheless, the findings indicate that the CAR-E treatment not only enhanced CAR T cell persistence but also improved the elimination of tumor cells.

The CAR-E enables therapy with a low dose of CAR T cells

Next, we conducted an experiment following a similar setting as described previously. However, in this study, we used a lower dose of only 100,000 CAR T cells (Fig. 3a). Notably, all mice treated with the BCMA–mutIL-2 CAR-E achieved complete tumor clearance ($n = 5$), whereas none of the control mice receiving either only CAR T cells ($n = 4$) or CAR T cells combined with VHH–mutIL-2 treatment ($n = 4$) were able to eliminate the tumors (Fig. 3b,c).

Analysis of blood samples collected at various time points revealed a robust expansion of CAR T cells in the circulation following the CAR-E treatment (Fig. 3d and Supplementary Fig. 6). This expansion resulted in elevated levels of interferon-γ (IFNγ) in the circulation (Supplementary Fig. 7a). Additionally, the treatment facilitated the generation of a diverse range of memory CAR T cells (Fig. 3e). The mice treated with the CAR-E exhibited no signs of toxicity according to clinical observations and weight measurements (Fig. 3h). Treatment with VHH–mutIL-2, while modestly improving the initial response compared to the no treatment group (Fig. 3c), did not induce significant expansion of CAR T cells in circulation (Fig. 3d) nor did it lead to the formation of memory CAR T cells in circulation (Fig. 3e). Although analyzed almost 2 weeks earlier than the CAR-E-treated cohort (day 41 compared to day 56), very few CAR T cells were detectable in the spleen or bone marrow of the VHH–mutIL-2-treated mice. In contrast, a substantial number

of CAR T cells with a diverse range of memory phenotypes were evident in the spleen and bone marrow of the CAR-E-treated mice almost 2 months after CAR T cell injection (Fig. 3f,g,i,j), consistent with our earlier experiments discussed in Fig. 2. These results further support the notion that the BCMA component of the CAR-E is essential for leading to a robust expansion of CAR T cells and guiding them to develop enduring memory cells.

Overall, these results underscore the efficacy of the BCMA–mutIL-2 CAR-E treatment in enhancing the clearance of tumor cells by CAR T cells and emphasize its potential in the generation of long-lasting memory cells.

The CAR-E leads to functional CAR T cells 3 months after infusion

Subsequently, we aimed to evaluate the long-term functionality of CAR T cells following treatment with the CAR-E. A similar experiment was conducted wherein mice received 1 million OPM2 cells followed by 0.5 million BCMA CAR T cells (Supplementary Fig. 8a). A group of mice received the CAR-E treatment (six doses, 200 µg per dose on days 4, 10, 14, 17, 21 and 28; $n = 5$). The control group received VHH–mutIL-2 treatment at the same dosage and schedule ($n = 5$), while an additional control cohort received only tumor cells ($n = 3$). As anticipated, all mice receiving CAR T cells exhibited an initial response compared to control mice without CAR T cells (Supplementary Fig. 8b). All the CAR-E-treated mice ($n = 5$) and three of five mice in the VHH–mutIL-2 group survived for 3 months, which encompassed the duration of the experiment (Supplementary Fig. 8b, day 77). The surviving mice were euthanized 3 months after injection of CAR T cells and the splenocytes and bone marrow cells were analyzed. The CAR-E-treated mice exhibited a significant abundance of CAR T cells homing and persisting in the bone marrow and spleen compared to mice receiving CAR T cells with the nontargeted low-affinity IL-2 (VHH–mutIL-2) treatment (Supplementary Fig. 8c), consistent with our previous results (Figs. 2 and 3). Given that there was a 2-month period of no treatment before the mice were euthanized, these results further suggest that the treatment facilitated the generation of memory cells among CAR T cells. To evaluate the functionality of the persisting CAR T cells in the CAR-E-treated mice, an in vitro killing assay was performed using the CAR T cells harvested from the bone marrow and spleen. These 3-month-old cells demonstrated efficient killing of tumor cells, indicating their sustained functionality in the long term (Supplementary Fig. 8d). Phenotypic analyses of the cells by flow cytometry revealed the presence of CAR T cells with memory phenotypes (Supplementary Figs. 8e and 9).

To gain deeper insights into the characteristics of the persisting CAR T cells, we performed single-cell RNA sequencing (scRNAseq) analysis on CAR^+ T cells isolated from mice treated with either the BCMA–mutIL-2 treatment or the VHH–mutIL-2 control. Despite the limited presence of CAR T cells in the VHH–mutIL-2-treated mice, a sufficient number of cells were obtained from one of the VHH-treated mice for the experiment (Supplementary Fig. 10a). The scRNAseq analysis revealed that the predominant population of persistent CAR T cells in the BCMA–mutIL-2-treated mouse consisted of $CD8^+$ T cells (Supplementary Fig. 10b,c), which exhibited an enrichment of genes associated with an activated T cell state (Supplementary Fig. 10d,e). This was evidenced by elevated expression levels of granzyme family genes, other cytotoxicity-associated genes and major histocompatibility complex (MHC) class II genes. No significant differences in activation markers were observed between CAR T cells obtained from the BCMA–mutIL-2-treated and VHH–mutIL-2-treated mice, as the mice had already cleared the tumors over 60 days earlier. Furthermore, the BCMA–mutIL-2 treatment did not induce the upregulation of exhaustion markers, indicating that the treatment did not induce exhaustion in the persisting CAR T cells. Additionally, the diversity of T cell receptor (TCR) clonotypes was evaluated in the BCMA–mutIL-2-treated and VHH–mutIL-2-treated mice (Supplementary Fig. 10f,g). Both groups displayed similar diversity in clonotypes present, suggesting that the BCMA–mutIL-2 CAR-E treatment could effectively facilitate the presence of a diverse TCR repertoire in persisting CAR T cells, as opposed to promoting the dominance of a restricted set of TCR clones.

Persisting CAR T cells retain the capacity to re-expand

To investigate the prolonged persistence of human CAR T cells and whether they retain the capacity to re-expand, we replicated the experiment using NSG mice lacking both class I and class II MHC molecules (referred to as NOD-*scid* H2-K1^{null} H2-Ab1^{null} H2-D1^{null} IL-2Rγ^{null} (NSG-MHC I/II double knockout (DKO)) mice). These mice demonstrate a delayed onset of graft-versus-host disease when exposed to human T cells. Furthermore, we examined whether the CAR-E remains effective when treatment was initiated 2 weeks after CAR T cell injection.

Accordingly, a similar experiment to that described in Supplementary Fig. 8 was conducted using NSG-DKO mice, with the CAR-E treatment being initiated on day 14 (Supplementary Fig. 11a). Regular BLI and blood analyses were used to assess tumor burden and CAR T cell expansion in circulation. The blood analyses indicated a robust expansion of CAR T cells in the CAR-E-treated group compared to the no treatment control group and, notably, all the CAR-E-treated mice ($n = 5$) cleared tumors, while three of the five control mice did (Supplementary Fig. 11b–e).

To assess the development of functional memory CAR T cells, all responding mice were rechallenged with 1 million OPM2 cells on day 91 after the injection of CAR T cells. In the CAR-E-treated cohort, four of five mice showed no tumor growth, while all three remaining control mice exhibited tumor growth (Supplementary Fig. 11b, day 101). Blood analyses after rechallenge revealed CAR T cell re-expansion in the circulation of the CAR-E-treated mice (Supplementary Fig. 11d,g). The only CAR-E-treated mouse that could not fully control the tumor growth did not show any CAR T cells in the circulation (M1 in Supplementary Fig. 11g).

Fig. 3 | The BCMA CAR-E enables treatment with a low dose of CAR T cells. **a**, Experimental setup. **b**,**c**, BLI analyses monitoring tumor burden in different groups (**b**), along with a survival analysis (**c**). The same quantification scale was used for all images (photons per second). **d**, Analyses of blood samples revealed that the CAR-E expands CAR T cells in the circulation. Data were analyzed with a one-way ANOVA on days 7, 14 and 21. Once all mice in the PBS cohort were euthanized, BCMA–mutIL-2 and VHH–mutIL-2 comparisons were performed with multiple Mann–Whitney U tests on days 28 and 35. Error bars represent the mean ± s.e.m. **e**, Analysis of blood samples showed the generation of memory CAR T cells in the BCMA–mutIL-2 group. Data were analyzed using uncorrected multiple Mann–Whitney U tests. Error bars represent the mean ± s.e.m. **f**,**g**, For the BCMA–mutIL-2 cohort, 2 months after CAR T cell injection, a substantial number of CAR T cells were detected in the spleen. In the 'CAR T cell + PBS' group, CAR T cells were detected in the spleen; however, these mice succumbed to tumor growth at around 20 days after CAR T cell injection. Data were analyzed by a two-way ANOVA with Tukey's multiple-comparisons test. Individual flow data are shown in Supplementary Fig. 6. Error bars represent the mean ± s.e.m. **h**, The treated mice maintained consistent body weight throughout the experiment. Error bars represent the mean ± s.e.m. **i**, Persisting CAR T cells in the BCMA–mutIL-2-treated mice's spleen exhibited a $CCR7^+CD45RA^+CD62L^+$ stem-cell memory phenotype, which was absent in the 'CAR T cell + VHH–mutIL-2' or 'CAR T cell + PBS' cohorts. **j**, tSNE plot displaying FlowSOM-defined clusters among persisting BCMA CAR T cells from BCMA–mutIL-2-treated mice (spleen and bone marrow) and VHH–mutIL-2-treated mice (only bone marrow). tSNE plot was based on surface marker expression of CD8α, CD4, CD45, CD45RA, CD45RO, CD62L, CD69, PD1, HLA-DR, CCR7 and BCMA CAR and revealed the presence of distinct memory T cell populations. CAR T cells were detected in the bone marrow of the VHH–mutIL-2-treated group but not the spleen. Further analyses are shown in Supplementary Fig. 7. The experiments in **a**–**j** used PBMCs from one donor; sample sizes were $n = 4$, 4 and 5 individual mice for PBS, VHH–mutIL-2 and BCMA–mutIL-2 groups, respectively.

https://doi.org/10.1038/s41587-024-02339-4

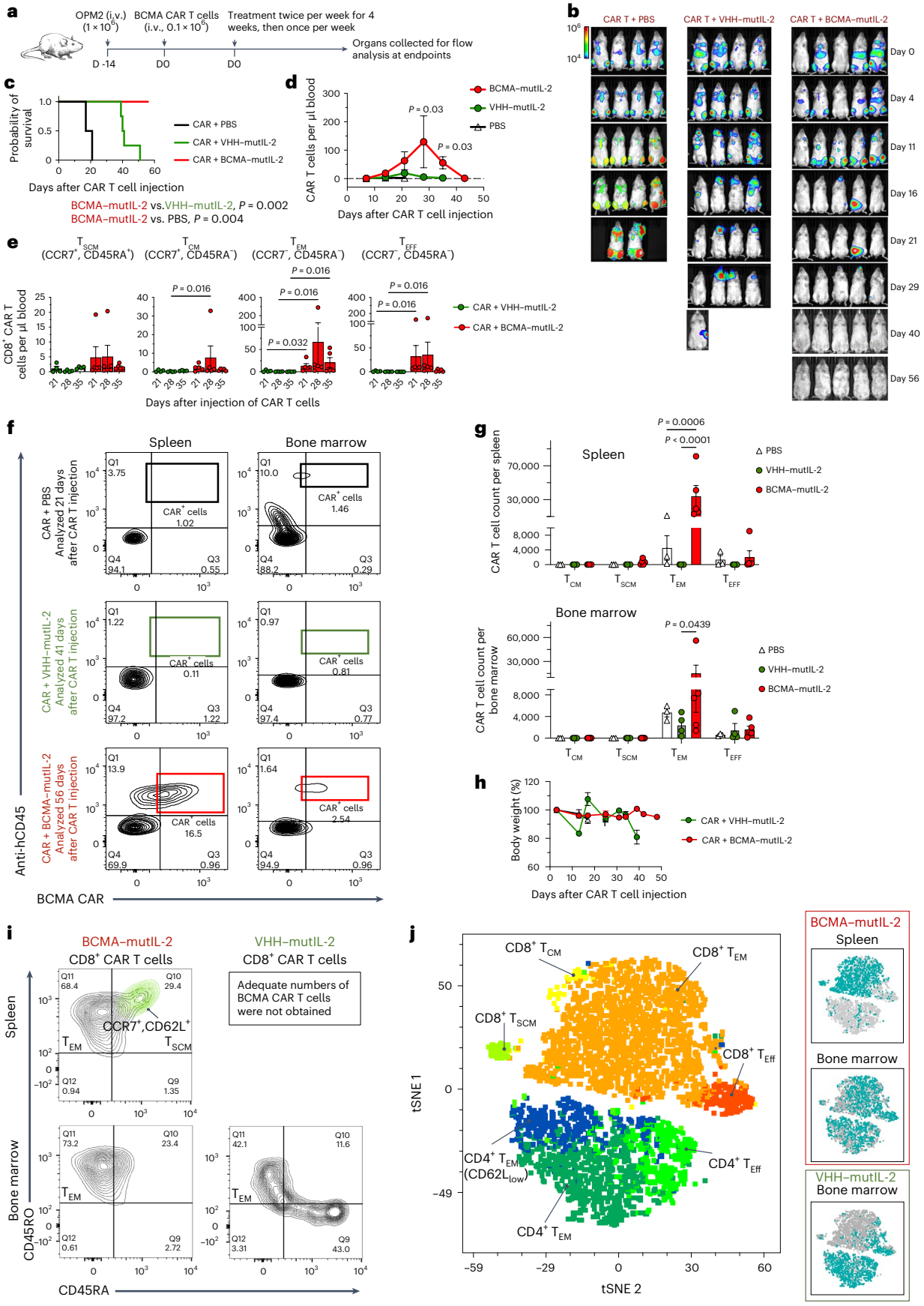

https://doi.org/10.1038/s41587-024-02339-4

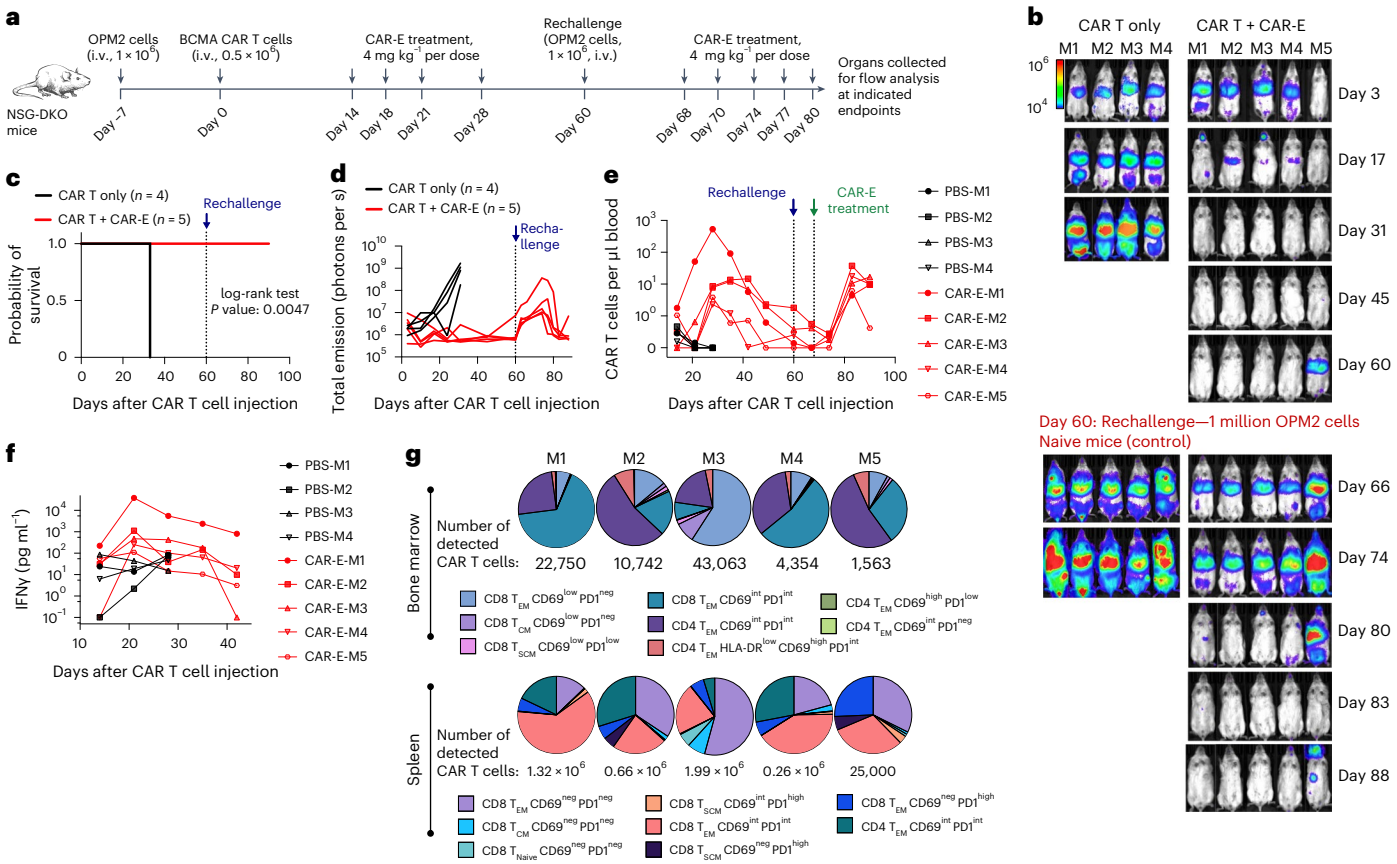

Fig. 4 | Lower doses of the CAR-E remain effective. The persisting CAR T cells retain the capacity to re-expand and control tumor growth upon rechallenge. a, Experimental setup ($n = 5$ for 'CAR T cell + CAR-E' cohort and $n = 4$ for 'CAR T cell only with no treatment' cohort). Surviving mice underwent rechallenge with 1 million OPM2 cells on day 60, followed by the CAR-E treatment on days 68, 70, 74, 77 and 80 at 4 mg kg^{-1}. Naive mice served as rechallenge controls. **b**, BLI monitored tumor burdens on the indicated days. The same BLI quantification scale was used for all images (photons per second). **c**, Survival analyses. All the CAR-E-treated mice survived for the duration of the experiment. Statistical analyses were conducted using the log-rank test (P value = 0.0047). **d**, Quantification of BLI analyses from **b**. **e**, Blood collected on the indicated days analyzed for CAR T cell presence in the circulation by flow cytometric analyses showed that CAR-E treatment robustly expanded CAR T cells in the circulation. The CAR-E treatment restarted on day 68 robustly re-expanded CAR T cells in the circulation. Individual data points for each mouse are presented. **f**, IFNγ levels were quantified using a multiplexed bead-based immunoassay on 1:25 diluted serum samples collected on the same days when CAR T cell counts were assessed as shown in **e**. **g**, At the endpoint, CAR T cells in the bone marrow and spleen of mice treated with the CAR-E showed a robust phenotypic diversity. Human CD45$^+$BCMA−CAR$^+$ cells from the bone marrow and spleen of mice were gated and concatenated. FlowSOM analysis was conducted on pooled populations to identify eight major phenotypic metaclusters. A heat map representing the mean fluorescence intensity of each marker within each metacluster was used to qualitatively describe each cluster (Supplementary Fig. 16). The proportion of each metacluster within the bone marrow and spleen of each mouse is depicted. The no treatment 'CAR T cell only' cohort did not have enough persisting CAR T cells in the bone marrow or spleen to allow for a similar analysis. The experiments in **a**–**g** used PBMCs from one donor; sample sizes were $n = 4$ and 5 individual mice for the CAR T only and CAR T + CAR-E groups, respectively.

To further challenge the persisting CAR T cells in the responder mice, a second rechallenge was conducted 144 days after the injection of CAR T cells (1 million OPM2 cells). Notably, no CAR-E treatment was administered between the first and second rechallenge (days 91 and 144). Two of four mice exhibited no tumor growth and the other two, while showing no signal in the bone marrow, showed a signal only in the liver, significantly lower than that of the control naive mice (Supplementary Fig. 11b, day 153). The two mice that fully controlled the growth of tumor cells in the second rechallenge showed the presence of stem-cell memory and naive CAR T cells in the circulation after the first rechallenge, suggesting that these are potentially the main CAR T cell subpopulations that allow re-expansion of the CAR T cells (M4 and M5 in Supplementary Fig. 11g).

On day 160, the remaining four mice treated with the CAR-E were euthanized and flow cytometric analyses of the organs revealed a significant presence of CAR T cells in the spleen and bone marrow (Supplementary Figs. 11h and 12). Notably, the bone marrow analysis at the endpoint indicated that the mouse in the CAR-E treatment group that exhibited a partial response to the initial rechallenge displayed a predominance of T_{EM} (CD45RA$^-$CD45RO$^+$CCR7$^-$) CD4$^+$ CAR T cells (M1 in the CAR-E group, Supplementary Fig. 11h). In contrast, the other four CAR-E-treated mice exhibited a diverse range of memory CAR T cell phenotypes, including C–C chemokine receptor 7 (CCR7)$^+$ cells (M2–M5 in the CAR-E group; Supplementary Fig. 11h). The control cohort displayed a less diverse population of CAR T cell phenotypes (Supplementary Fig. 11h).

A lower frequency of the CAR-E treatment remains effective

Next, we conducted an experiment to investigate the efficacy of a reduced frequency of the CAR-E treatment initiated 2 weeks after CAR T cell injection, as shown in Fig. 4a. The treatment group received four doses of the CAR-E treatment (4 mg kg^{-1} per dose) on days 14, 18, 21 and 28 (Fig. 4a).

Bioluminescence imaging (BLI) analyses demonstrated that all mice ($n = 5$) receiving the CAR-E cleared tumors, while none of the control mice ($n = 4$) achieved tumor clearance (Fig. 4b–d). Blood analyses

https://doi.org/10.1038/s41587-024-02339-4

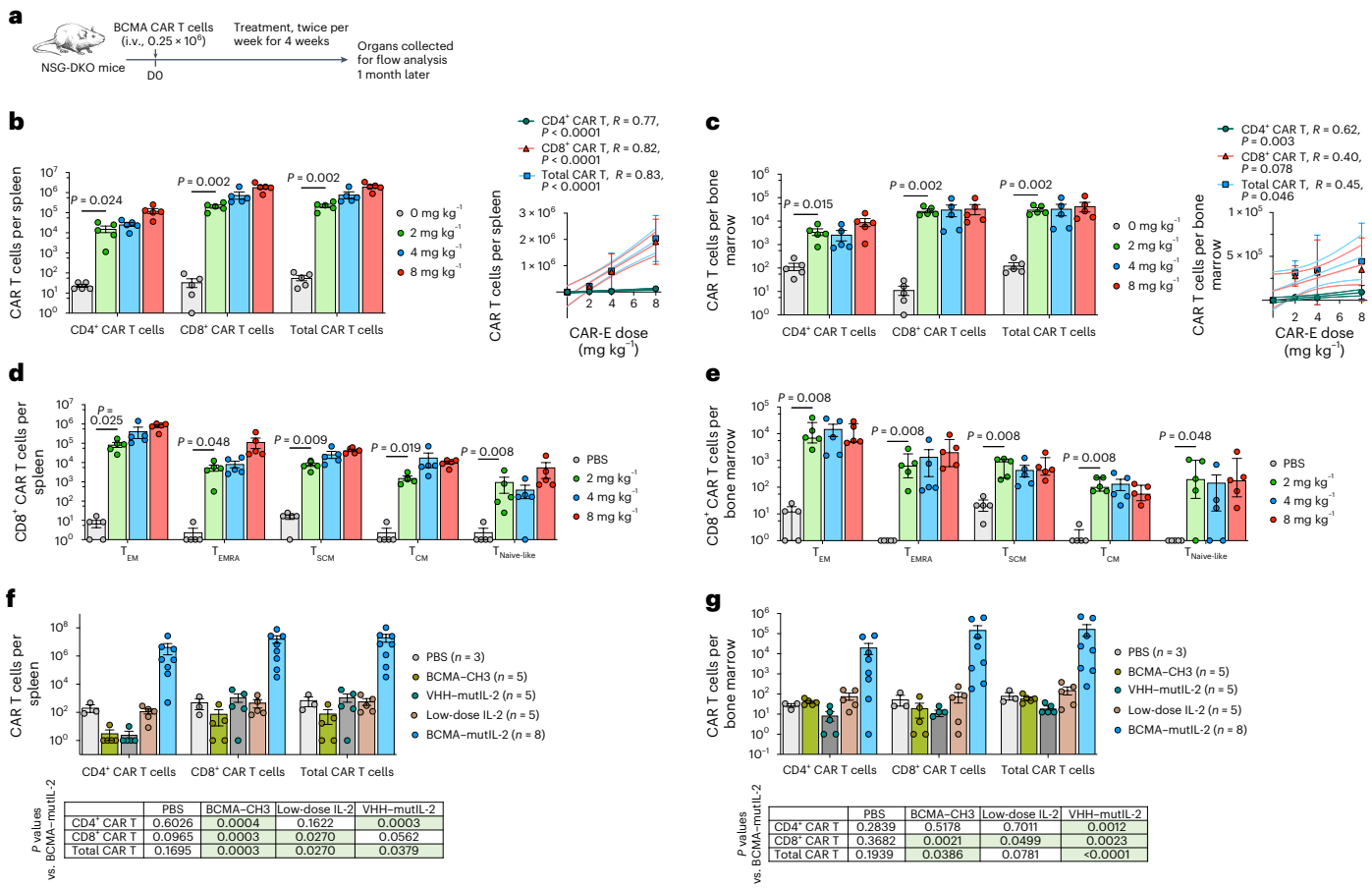

Fig. 5 | The CAR-E expands CAR T cells in the absence of tumor cells in a dose-dependent manner. a, Experimental setup. Mice received varying doses of the BCMA–mutIL-2 CAR-E treatment ($n = 5$ for each cohort). **b**,**c**, Spleen (**b**) and bone marrow (**c**) were isolated 30 days after the injection of CAR T cells and CAR$^+$ cells were counted by flow cytometric analyses. Left: column bars indicating the absolute number of detected CAR T cells. Right: statistical analyses demonstrate that the CAR-E leads to dose-dependent expansion of CAR T cells. The significance between the PBS group and the group of mice receiving the lowest treatment dose (2 mg kg^{-1}) was measured using a two-sided unpaired *t*-test. Additionally, a linear regression was conducted to demonstrate the dose-dependent effect of the treatment, where error bars represent the mean ± 95% CI. **d**,**e**, Persisting CAR T cells consisted of different subsets of memory T cells in the spleen (**d**) and bone marrow (**e**). T_{EM} cells, CD45RA$^-$CD45RO$^+$CCR7$^-$; T_{EMRA} cells, CD45RA$^+$CD45RO$^+$CCR7$^-$; T_{SCM} cells, CD45RA$^+$CD45RO$^+$CCR7$^+$; T_{CM} cells, CD45RA$^-$CD45RO$^+$CCR7$^+$; $T_{Naive\text{-}like}$ cells, CD45RA$^+$CD45RO$^-$CCR7$^+$. In **d**,**e**, we used the Shapiro–Wilk test to assess normality. Normal datasets were analyzed using an unpaired two-sided *t*-test, while non-normal datasets were analyzed using a Mann–Whitney U test. The experiments in **a**–**e** used PBMCs from one donor, with all conditions having $n = 5$, where n represents individual mice. **f**, Both the antigen and the low-affinity IL-2 components of the CAR-E are essential for its impact. Mice received CAR T cells and different treatments (4 mg kg^{-1}) following a schedule similar to that shown in **a**. The BCMA–CH3 antigen, VHH–mutIL-2 or low-dose wild-type IL-2 treatments could not result in the expansion or persistence of CAR T cells. The experiments in **f**,**g** used PBMCs from two donors. A Kruskal–Wallis test was used for each subset of CAR T cells and total T cells. Subsequently, a post hoc Dunn's analysis was conducted to compare each group with the treatment group. The table below the graph displays the adjusted *P* values. Error bars represent the mean ± s.e.m. for all box plots.

indicated that the four doses of the CAR-E treatment were sufficient to robustly expand CAR T cells in all the treated mice compared to the control cohort (Fig. 4e and Supplementary Fig. 14). Cytokine assessments also revealed elevated levels of IFNγ in the CAR-E treatment cohort (Fig. 4f).

One of the CAR-E-treated mice (M5) showed liver relapse on day 60 (Fig. 4b). Regardless, all five CAR-E-treated mice underwent tumor rechallenge on day 60. All mice showed a considerably lower signal compared to the control naive mice (Fig. 4b, day 66). While the mice exhibited liver signals, none showed bone marrow signals, suggesting the presence of functional memory CAR T cells in the bone marrow. To investigate whether the CAR-E treatment could prompt CAR T cell re-expansion and control tumor growth in liver metastasis, mice were retreated with the CAR-E (4 mg kg^{-1}) on days 68, 70, 74, 77 and 80. All mice successfully cleared the liver metastasis (Fig. 4b, day 83). The mouse that showed relapse on day 60 (M5, Fig. 4b) also cleared the tumor, although it exhibited some signal on the last day of the experiment. Blood analyses confirmed that the CAR-E resulted in a robust re-expansion of the CAR T cells (Fig. 4e). Flow cytometric analyses on day 90 revealed the presence of CAR T cells with diverse memory phenotypes (Fig. 4g and Supplementary Fig. 15).

In summary, the results indicated that the BCMA CAR-E not only facilitated the complete clearance of tumor cells but also promoted the formation of functional memory CAR T cells.

The CAR-E expands CAR T cells in the absence of tumor antigens

We hypothesized that the CAR-E mechanism of action is independent of tumor cells. To test this, mice were solely injected with 0.25 million BCMA CAR T cells in the absence of tumor cells. Additionally, to simultaneously assess whether the CAR-E impact is dose dependent, we assigned mice to different cohorts receiving varying doses of the BCMA–mutIL-2 CAR-E treatment (Fig. 5a). Organs were collected 1 month later and assessed using flow cytometric analyses.

As expected, the CAR-E treatment resulted in the expansion and persistence of CAR T cells in the spleen and bone marrow (Fig. 5b,c and Supplementary Fig. 17). Furthermore, the results demonstrated that the CAR-E impact on CAR T cells is dose dependent (Fig. 5b,c). Even at the lowest tested dose of 2 mg kg^{-1}, there were a substantial number of persisting CAR T cells compared to the no treatment cohort (Fig. 5b,c). Additional analyses indicated that the CAR-E induced the generation of memory CAR T cells (Fig. 5d,e).

To confirm the essential role of the low-affinity IL-2 component of the CAR-E, a similar experiment, as described above, was repeated using the 4 mg kg^{-1} dose and 0.25 million CAR T cells. Mice received the BCMA–mutIL-2 CAR-E treatment, the BCMA–CH3 molecule or no treatment. As anticipated, the antigen-only BCMA–CH3 treatment cohort did not result in the expansion or persistence of CAR T cells, further validating that both the BCMA and the low-affinity IL-2 components of the CAR-E are necessary for its impact on CAR T cells (Fig. 5f,g and Supplementary Fig. 18). This aligns with our previous in vitro and in vivo analyses (Figs. 1, 2 and 3). A cohort that received low-dose IL-2 also failed to result in substantial persisting CAR T cells (Fig. 5f,g). Furthermore, as expected, the nontargeted low-affinity IL-2 (VHH–mutIL-2) did not lead to the expansion or persistence of CAR T cells (Fig. 5f,g), consistent with our prior findings discussed in Figs. 1, 2 and 3 and Supplementary Fig. 11.

In summary, these findings demonstrate that the CAR-E can expand CAR T cells and promote the development of diverse memory phenotypes, regardless of the presence of tumor cells. Both the BCMA and the low-affinity IL-2 component of the CAR-E are necessary for its efficacy.

The CAR-E requires engagement of both IL-2R and CAR (4-1BB–CD3ζ) endodomain

To better understand the mechanism of action of the CAR-E, we investigated whether its effect on CAR T cells is solely mediated by anchoring the low-affinity IL-2 onto CAR T cells through BCMA-to-CAR binding or whether it involves simultaneous engagement of both IL-2R and CAR endodomains. For this purpose, CAR T cells were made using a construct lacking the 4-1BB–CD3ζ intracellular endodomain but retaining an identical extracellular ectodomain (referred to as CAR intracellular domain deletion or CAR-ICD-Δ). In vitro analyses demonstrated that the BCMA–mutIL-2 CAR-E induced pSTAT5 in CAR-ICD-Δ T cells, similar to full CAR T cells (Fig. 6a), suggesting that the effects of low-affinity IL-2 were similar in both CAR constructs and were mediated by antigen-to-CAR binding.

However, while the CAR-E robustly activated full CAR T cells, as evidenced by elevated CD69 expression and increased production of IFNγ and tumor necrosis factor-α (TNFα), its impact on CAR T cells with the CAR-ICD-Δ construct was negligible (Fig. 6b–d). Dasatinib, a protein kinase Lck inhibitor, and ruxolitinib, a Janus kinase inhibitor, both individually and in combination, significantly inhibited the impact of the CAR-E (Fig. 6e–g), further suggesting that the CAR-E engages both CAR and IL-2R endodomains. Subsequently, we compared the in vivo impact of the CAR-E on full CAR and CAR-ICD-Δ T cells. Mice injected with 0.25 million CAR T cells in the absence of tumor cells received CAR-E treatments (4 mg kg^{-1} twice per week for 4 weeks; Fig. 6h). After 1 month, animals were euthanized and their organs were analyzed by flow cytometry. While the CAR-E robustly expanded CAR T cells with the full CAR construct, consistent with our previous results, it did not result in the expansion or persistence of CAR-ICD-Δ T cells (Fig. 6i).

To gain additional insights into the mechanism of action of the CAR-E, we investigated its impact on the transcriptome of CAR T cells. Various treatments, including BCMA–mutIL-2 CAR-E, VHH–mutIL-2, BCMA–CH3 antigen and wild-type IL-2, were added to CAR T cells. As an additional control, CAR-ICD-Δ T cells were treated with the BCMA–mutIL-2 CAR-E. Treatments were removed after 2 h to mimic in vivo conditions and cells were subjected to bulk RNAseq 2 or 22 h later.

The CAR-E induced substantial transcriptomic changes, demonstrating quantitatively larger fold changes compared to all other conditions, including wild-type IL-2 (Fig. 6j–n). The differences in gene upregulation of the BCMA–mutIL-2 compared to wild-type IL-2, VHH–mutIL-2 and BCMA–CH3, as well as the gene set enrichment analysis of these different conditions (Supplementary Fig. 19), showed that, while these control treatments had an effect on their own, the stimulation induced by the CAR-E was greatly superior (Fig. 6l,m). The impact of the CAR-E on CAR-ICD-Δ T cells was mild, further emphasizing the essential role of the CAR endodomain in the CAR-E's mechanism of action (Fig. 6j,k).

In summary, these findings indicate that the mechanism of action of the CAR-E goes beyond merely delivering low-affinity IL-2 to CAR T cells. Instead, it operates by engaging both the CAR endodomain and IL-2R molecules.

Discussion

Relapse remains a major concern in persons with MM receiving BCMA CAR T cells. Most relapses are associated with BCMA-expressing tumors[8], indicating that CAR T cell functionality and persistence must be augmented. In this study, we address this critical clinical shortcoming by developing the CAR-E approach, which delivers an enhancer molecule to CAR T cells. We showed that a BCMA CAR-E consisting of the BCMA ectodomain fused to a low-affinity IL-2 enhances the activity and persistence of BCMA CAR T cells.

Our results demonstrate that the CAR-E engages both IL-2R and the CAR endodomains. Inhibiting either signaling pathway reduces the impact of the CAR-E. The CAR-E loses its effect on CAR T cells lacking a CAR endodomain. The antigen alone modestly activates CAR T cells at high concentrations in vitro and cannot expand CAR T cells in vivo, highlighting the essential role of the low-affinity IL-2 component in the CAR-E's mechanism of action. Similarly, treatment with the nontargeted low-affinity IL-2 (VHH–mutIL-2) cannot mimic the effects observed with the BCMA–mutIL-2, emphasizing the indispensable role of the antigen in the CAR-E mechanism of action. The slower internalization rate of the CAR-E compared to free IL-2 results in prolonged IL-2 signaling, which could be pivotal to its potency despite a brief circulatory half-life. Costimulatory molecules in the CAR endodomain, such as 4-1BB or CD28, may contribute differently to the CAR-E mechanism of action.

The generation of memory CAR T cells has been a longstanding challenge in the field. Our results demonstrate that the CAR-E can guide CAR T cells in developing memory cells with diverse phenotypes and it can do so independently of the presence of tumor cells. The CAR-E leads to the generation of a spectrum of different memory subtypes, including stem-cell memory populations. This diversity is likely responsible for the observed long-term persistence of CAR T cells that retain the capacity to re-expand upon restimulation. This capability of the CAR-E may be attributable to its mechanism of action, simultaneously engaging both IL-2R and CAR (4-1BB–CD3ζ) endodomains.

Incorporating a full-size (inactive) Fc molecule would greatly extend the circulatory half-life to several days because of FcRn recycling. However, pulsing CAR T cells with the CAR-E is likely superior to prolonged exposure, which may lead to exhaustion or the generation of terminally differentiated CAR T cells. Therefore, a CAR-E with a short half-life is expected to be more effective in promoting the generation of memory CAR T cells. Additionally, this reduces potential competition with tumor antigens for CAR binding. While one dose of an Fc-based CAR-E may result in uncontrolled expansion of CAR T cells, a single dose of a CAR-E with a short half-life is unlikely to result in uncontrollable CAR T cell proliferation, thereby enhancing the safety profile in patients. Therefore, we opted to use the CH3 domain of IgG1 as the spacer for CAR-E molecules.

The CAR-E approach can be generalized to deliver diverse immune-modulating molecules to CAR T cells to enhance their activity

https://doi.org/10.1038/s41587-024-02339-4

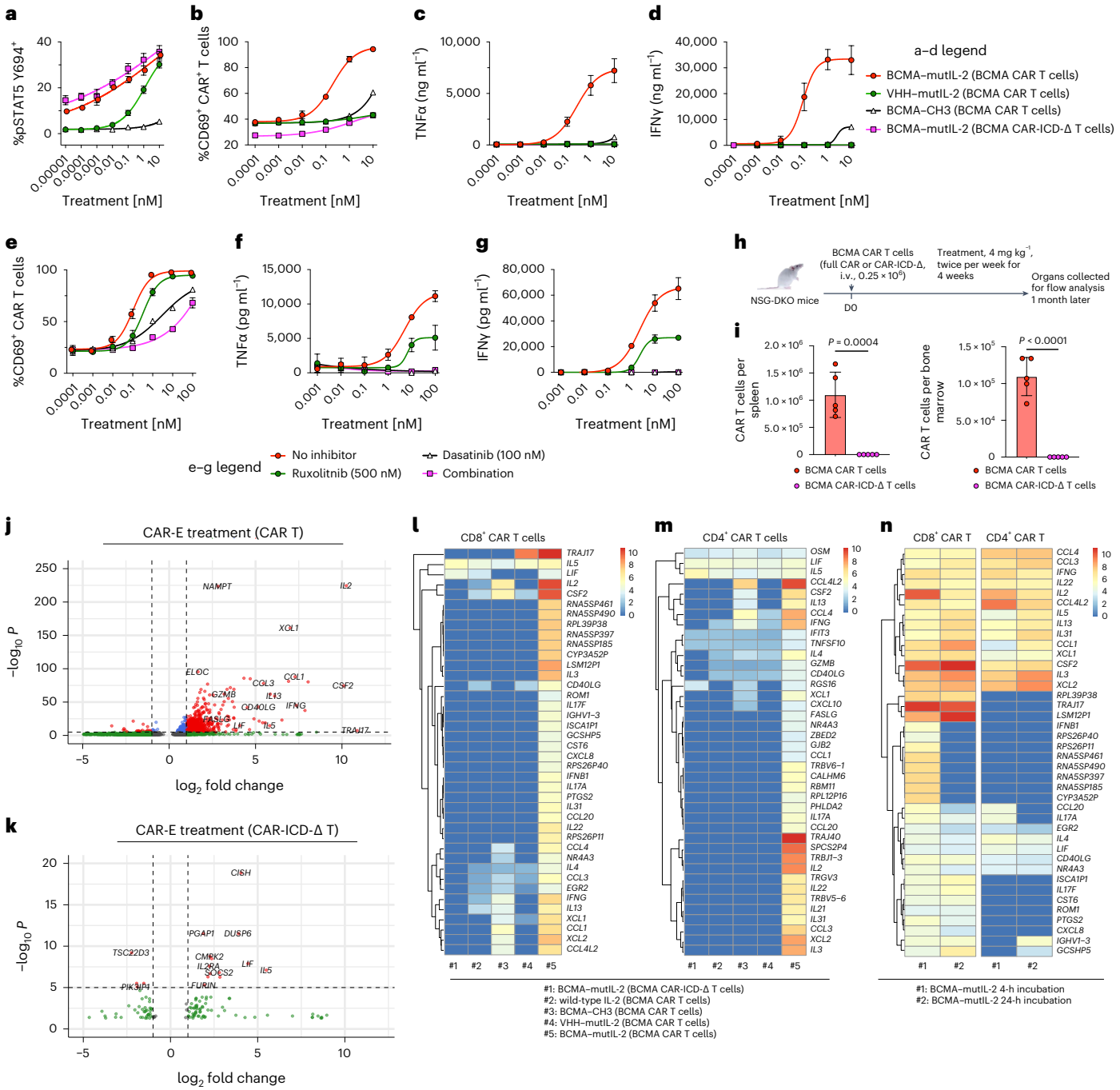

Fig. 6 | The CAR-E induces substantial transcriptomic changes in CAR T cells and its efficacy requires signaling through both the CAR and the IL-2R endodomains. a, The CAR-E induces pSTAT5 activity similarly in CAR T cells and CAR-ICD-Δ T cells. Error bars represent the mean ± s.d. **b**–**d**, The CAR-E activates CAR T cells but almost completely loses its impact on CAR-ICD-Δ T cells, as evidenced by lower CD69 expression levels (**b**) and reduced induction of IFNγ (**c**) and TNFα (**d**) production. Error bars represent the mean ± s.d. The experiment used PBMCs from one donor. In **a**–**d**, $n = 3$ technical replicates for each condition. **e**–**g**, Dasatinib and ruxolitinib decrease the impact of the CAR-E on CAR T cells, as demonstrated by decreased CD69 expression levels (**e**) and reduced IFNγ (**f**) and TNFα (**g**) production. CAR T cells were treated with varying doses of the CAR-E treatment and the individual inhibitor or their combination, with assessments conducted 24 h later ($n = 3$ technical replicates for each point). Error bars represent the mean ± s.d. **h**,**i**, The CAR-E cannot expand CAR-ICD-Δ T cells in vivo. The experimental setup is shown in **h** ($n = 5$ mice per group). Organ analyses 1 month after the injection of cells revealed significant persistence of full CAR T cells, while no CAR-ICD-Δ T cells could be detected (**i**). The experiment used PBMCs from one donor. Data are presented as the mean ± s.d. and were analyzed by a two-sided unpaired *t*-test. **j**–**n**, The CAR-E rapidly induces substantial transcriptomic changes in CAR T cells. CAR T cells underwent a 2-h incubation with the BCMA–mutIL-2 CAR-E or control molecules (10 nM), followed by treatment removal. Subsequently, RNAseq was performed 2 and 24 h later. A volcano plot showing the highest upregulated genes at 4 h when CD8+ CAR T cells were treated with the CAR-E (**j**). A volcano plot showing that the BCMA–mutIL-2 CAR-E has a negligible impact on CD8+ CAR-ICD-Δ T cells (**k**). *P* values were obtained using a Wald test (**j**,**k**). **l**–**n**, The top 40 upregulated genes are displayed for the CAR-E treatment for CD8+ CAR T cells (**l**) and CD4+ CAR T cells (**m**). The treatment conditions in both CD4 and CD8 CAR T cells, at 2 and 24 h (**n**). Additional RNAseq analyses are included in Supplementary Fig. 19.

and trafficking. Although the low-affinity IL-2 molecule serves as an excellent enhancer, other enhancer molecules should be investigated, especially for long-term efficacy (>6–12 months after the injection of CAR cells). For example, evaluating the inclusion of IL-7, IL-12, IL-15 and IL-21 in CAR-E design is worth pursuing. It is also possible to deliver inhibitory molecules to CAR T cells to decrease their activity as needed and potentially in a reversible manner. Currently, persons with MM receive BCMA CAR T cell therapy after failing to respond to other treatments, including chemotherapy, which may lower T cell quality. While most persons with MM exhibit a promising initial response to CAR T cell therapy, investigating the effects of the CAR-E on patient-derived T cells could shed light on the CAR-E's impact on CAR T cells with potentially lower initial quality compared to those derived from healthy donors.

Several studies have reported that the baseline levels of soluble BCMA do not influence a person's response to BCMA CAR therapy[3,34–36]. Our extensive in vitro and in vivo data demonstrate that the CAR-E does not hinder CAR T cell activity. This is likely attributable to the higher-affinity binding of membrane-bound antigen to CAR molecules resulting from the formation of a tumor–T cell synapse, the dynamic nature of interactions between the CAR and CAR-E molecules and the short half-life and intermittent dosing of the CAR-E treatment.

The CAR-E approach can also be adapted to CAR T cells directed at other liquid tumors, such as CD19 or CD22 CAR T cells, or solid tumors, such as glypican 3, mesothelin or human epidermal growth factor receptor 2 CAR T cells. Furthermore, the approach has the potential to enhance the activity and persistence of CAR natural killer cells.

The expansion of CAR T cells by the CAR-E treatment may offer the possibility of reducing or even eliminating lymphodepleting chemotherapy as a preconditioning regimen. Lymphodepletion typically results in an increased concentration of homeostatic, T cell-stimulating cytokines such as IL-7 and IL-15 (ref. 37). By selectively delivering IL-2 to CAR T cells, the CAR-E could bypass the need for lymphodepletion, as IL-2 and IL-15 use the same receptors for signaling.

A major challenge of CAR T cell therapy relates to pharmacokinetics, namely, an initial massive expansion followed by a sharp drop-off in CAR T cell numbers. Massive T cell expansion leads to cytokine release syndrome (CRS) because of the activation of T cells leading to cytokine release, in turn activating other immune effector cells such as monocytes and macrophages, which further elaborate inflammatory cytokines within the first 1–2 weeks after CAR T cell infusion. The sharp drop-off after initial expansion is because of a failure of T cells to persist, increasing the likelihood of disease relapse. Current genetic engineering approaches aimed at improving CAR T cell persistence may intensify initial expansion, exacerbating CRS. In contrast, the CAR-E approach promotes T cell persistence even after tumor antigen clearance and at a desired time point. For instance, the CAR-E initiation could occur several weeks after CAR T cell injection, well beyond the CRS window. Moreover, the short half-life of CAR-E molecules and intermittent dosing reduce the risk of the CAR-E-induced CRS occurrence.

Our evaluation of the CAR-E treatment involved assessing its potency and side-effect profile in human CAR T cells and human xenograft models in immunodeficient mice. The limited cross-reactivity of human cytokines in mice restricted our ability to fully evaluate the CAR-E-mediated immune-related adverse events. Therefore, careful clinical testing of the CAR-E treatment is needed to determine whether the resulting expansion and persistence of CAR T cells are well tolerated after tumor reduction.

The potential for immunogenicity with the CAR-E is minimal because of its nearly fully self-human protein construct, with only two point substitutions in the IL-2 component and G_4S linkers between the components. Persons with MM, who exhibit elevated levels of BCMA soluble antigen, have not reported immunogenicity associated with BCMA protein. However, the immunogenicity issue requires evaluation in nonhuman primates and phase 1 trials. Even if the CAR-E shows immunogenicity in some persons, it is unlikely to compromise CAR T cell activity, as shown in Fig. 1e. Furthermore, the short half-life enhances the safety profile, with the CAR-E rapidly clearing from circulation.

In summary, the CAR-E robustly enhances CAR T cell activity and persistence and drives the generation of a diverse range of memory subpopulations of CAR T cells that retain the capacity to re-expand upon restimulation. The CAR-E approach offers an opportunity to selectively target CAR T cells after infusion and deliver immunomodulatory molecules to their cell surface. The approach does not require additional engineering of CAR T cells and can be integrated with Food and Drug Administration-approved or newer generations of CAR cells.

Online content

Any methods, additional references, Nature Portfolio reporting summaries, source data, extended data, supplementary information, acknowledgements, peer review information; details of author contributions and competing interests; and statements of data and code availability are available at https://doi.org/10.1038/s41587-024-02339-4.

References

1. Turtle, C. J. et al. CD19 CAR-T cells of defined $CD4^+$:$CD8^+$ composition in adult B cell ALL patients. *J. Clin. Invest.* **126**, 2123–2138 (2016).
2. Roex, G. et al. Safety and clinical efficacy of BCMA CAR-T-cell therapy in multiple myeloma. *J. Hematol. Oncol.* **13**, 164 (2020).
3. Raje, N. et al. Anti-BCMA CAR T-cell therapy bb2121 in relapsed or refractory multiple myeloma. *N. Engl. J. Med.* **380**, 1726–1737 (2019).
4. Hartmann, J., Schüßler-Lenz, M., Bondanza, A. & Buchholz, C. J. Clinical development of CAR T cells—challenges and opportunities in translating innovative treatment concepts. *EMBO Mol. Med.* **9**, 1183–1197 (2017).
5. Lindner, S. E., Johnson, S. M., Brown, C. E. & Wang, L. D. Chimeric antigen receptor signaling: functional consequences and design implications. *Sci. Adv.* **6**, eaaz3223 (2020).
6. Amini, L. et al. Preparing for CAR T cell therapy: patient selection, bridging therapies and lymphodepletion. *Nat. Rev. Clin. Oncol.* **19**, 342–355 (2022).
7. Deng, H. et al. Efficacy of humanized anti-BCMA CAR T cell therapy in relapsed/refractory multiple myeloma patients with and without extramedullary disease. *Front. Immunol.* **12**, 720571 (2021).
8. Rodriguez-Otero, P. et al. Ide-cel or standard regimens in relapsed and refractory multiple myeloma. *N. Engl. J. Med.* **388**, 1002–1014 (2023).
9. Zhou, X., Rasche, L., Kortüm, K. M., Mersi, J. & Einsele, H. BCMA loss in the epoch of novel immunotherapy for multiple myeloma: from biology to clinical practice. *Haematologica* **108**, 958–968 (2022).
10. San-Miguel, J. et al. Cilta-cel or standard care in lenalidomide-refractory multiple myeloma. *N. Engl. J. Med.* **389**, 335–347 (2023).
11. Weinkove, R., George, P., Dasyam, N. & McLellan, A. D. Selecting costimulatory domains for chimeric antigen receptors: functional and clinical considerations. *Clin. Transl. Immunol.* **8**, e1049 (2019).
12. Dai, Q. et al. 4-1BB signaling boosts the anti-tumor activity of CD28-incorporated 2nd generation chimeric antigen receptor-modified T cells. *Front. Immunol.* **11**, 539654 (2020).
13. Majzner, R. G. et al. Tuning the antigen density requirement for CAR T-cell activity. *Cancer Discov.* **10**, 702–723 (2020).
14. Cheng, Z. et al. In vivo expansion and antitumor activity of coinfused CD28- and 4-1BB-engineered CAR-T cells in patients with B cell leukemia. *Mol. Ther.* **26**, 976–985 (2018).
15. Drent, E. et al. Combined CD28 and 4-1BB costimulation potentiates affinity-tuned chimeric antigen receptor-engineered T cells. *Clin. Cancer Res.* **25**, 4014–4025 (2019).

16. Cherkassky, L. et al. Human CAR T cells with cell-intrinsic PD-1 checkpoint blockade resist tumor-mediated inhibition. *J. Clin. Invest.* **126**, 3130–3144 (2016).
17. Rupp, L. J. et al. CRISPR/Cas9-mediated PD-1 disruption enhances anti-tumor efficacy of human chimeric antigen receptor T cells. *Sci. Rep.* **7**, 737 (2017).
18. Fraietta, J. A. et al. Disruption of *TET2* promotes the therapeutic efficacy of CD19-targeted T cells. *Nature* **558**, 307–312 (2018).
19. Feucht, J. et al. Calibration of CAR activation potential directs alternative T cell fates and therapeutic potency. *Nat. Med.* **25**, 82–88 (2019).
20. Agarwal, S. et al. Deletion of the inhibitory co-receptor CTLA4 enhances and invigorates chimeric antigen receptor T cells. *Immunity* **56**, 2388–2407 (2023).
21. Hu, B. et al. Augmentation of antitumor immunity by human and mouse CAR T cells secreting IL-18. *Cell Rep.* **20**, 3025–3033 (2017).
22. Chmielewski, M. & Abken, H. C. A. R. T. Cells releasing IL-18 convert to T-Bet^{high} FoxO1^{low} effectors that exhibit augmented activity against advanced solid tumors. *Cell Rep.* **21**, 3205–3219 (2017).
23. Hurton, L. V. et al. Tethered IL-15 augments antitumor activity and promotes a stem-cell memory subset in tumor-specific T cells. *Proc. Natl Acad. Sci. USA* **113**, E7788–E7797 (2016).
24. Kueberuwa, G., Kalaitsidou, M., Cheadle, E., Hawkins, R. E. & Gilham, D. E. CD19 CAR T cells expressing IL-12 eradicate lymphoma in fully lymphoreplete mice through induction of host immunity. *Mol. Ther. Oncolytics* **8**, 41–51 (2018).
25. Hawkins, E. R., D'Souza, R. R. & Klampatsa, A. Armored CAR T-cells: the next chapter in T-cell cancer immunotherapy. *Biologics* **15**, 95–105 (2021).
26. Mohammed, S. et al. Improving chimeric antigen receptor-modified T cell function by reversing the immunosuppressive tumor microenvironment of pancreatic cancer. *Mol. Ther.* **25**, 249–258 (2017).
27. Wang, Y. et al. An IL-4/21 inverted cytokine receptor improving CAR-T cell potency in immunosuppressive solid-tumor microenvironment. *Front. Immunol.* **10**, 1691 (2019).
28. Sockolosky, J. T. et al. Selective targeting of engineered T cells using orthogonal IL-2 cytokine–receptor complexes. *Science* **359**, 1037–1042 (2018).
29. Ma, L. et al. Enhanced CAR-T cell activity against solid tumors by vaccine boosting through the chimeric receptor. *Science* **365**, 162–168 (2019).
30. Reinhard, K. et al. An RNA vaccine drives expansion and efficacy of claudin-CAR-T cells against solid tumors. *Science* **367**, 446–453 (2020).
31. Quayle, S. N. et al. CUE-101, a novel E7–pHLA–IL2–Fc fusion protein, enhances tumor antigen-specific T-cell activation for the treatment of HPV16-driven malignancies. *Clin. Cancer Res.* **26**, 1953–1964 (2020).
32. Cibrián, D. & Sánchez-Madrid, F. CD69: from activation marker to metabolic gatekeeper. *Eur. J. Immunol.* **47**, 946–953 (2017).
33. Yu, A., Olosz, F., Choi, C. Y. & Malek, T. R. Efficient internalization of IL-2 depends on the distal portion of the cytoplasmic tail of the IL-2R common γ-chain and a lymphoid cell environment. *J. Immunol.* **165**, 2556–2562 (2000).
34. Ali, S. A. et al. T cells expressing an anti-B-cell maturation antigen chimeric antigen receptor cause remissions of multiple myeloma. *Blood* **128**, 1688–1700 (2016).
35. Cohen, A. D. et al. B cell maturation antigen-specific CAR T cells are clinically active in multiple myeloma. *J. Clin. Invest.* **129**, 2210–2221 (2019).
36. Mailankody, S. et al. Orvacabtagene autoleucel (orva-cel), a B-cell maturation antigen (BCMA)-directed CAR T cell therapy for patients (pts) with relapsed/refractory multiple myeloma (RRMM): update of the phase 1/2 EVOLVE study (NCT03430011). *J. Clin. Oncol.* **38**, 8504 (2020).
37. Kochenderfer, J. N. et al. Lymphoma remissions caused by anti-CD19 chimeric antigen receptor T cells are associated with high serum interleukin-15 levels. *J. Clin. Oncol.* **35**, 1803–1813 (2017).

Methods

Cell lines and culture

PBMCs were obtained by Ficoll gradient of apheresis leukoreduction collars of healthy platelet donors. HEK293T cells were cultured in complete DMEM (Gibco), 1% L-glutamine (Gibco), 1% nonessential amino acids (Gibco), 1% pyruvate (Gibco), 1% penicillin and streptomycin (Cytiva) and 10% FBS (Biowest). OPM2 cells and PBMCs were cultured in complete RPMI-1640 medium (Gibco), 1% L-glutamine (Gibco), 1% nonessential amino acids (Gibco), 1% pyruvate (Gibco), 1% penicillin and streptomycin (Cytiva) and 10% FBS (Biowest). All cells were grown in 5% CO_2, 95% air-humidified incubators at 37 °C. OPM2 cells were genetically engineered to express GFP and firefly luciferase. Liver-derived and bone marrow-derived OPM2 cells were obtained from metastatic lesions in the bone marrow and liver of a mouse injected with OPM2 cells. Bone marrow-derived cells were used in experiments detailed in Figs. 3, 4 and 6h and Supplementary Fig. 11 and liver-derived OPM2 cells were used in rechallenge experiments detailed in Fig. 4 and Supplementary Fig. 11.

Mouse studies

All experiments adhered to the pertinent ethical and safety protocols. The studies were carried out under the oversight of the Dana-Farber Cancer Institute Institutional Animal Care and Use Committee (IACUC; protocol number 20-006) and the Boston Children's Hospital Committee on Animal Care (protocol number BCH 00001455). Our study did not involve research with human subjects, as no personal or specific information was required for the human PBMCs obtained from healthy donors. The xenograft models used were described previously[38]. Briefly, 5–8-week-old NSG and NSG-DKO mice were either purchased from Jackson Laboratory or bred in-house. All mice were sex-matched and age-matched into groups. Xenograft models were established by intravenous injection of 1×10^6 OPM2 cells expressing GFP and luciferase in 200 µl of PBS. Mice received indicated treatments in 300 µl of PBS through intraperitoneal (i.p.) injections. Tumor burden was assessed using the IVIS Lumina Series III (Perkin Elmer) after i.p. injection of D-luciferin (200 µl, from a 15 mg ml^{-1} solution; 2-min imaging). BLI intensity was analyzed by Aura imaging analysis software (Spectral Instruments Imaging). Peripheral blood from mice was obtained by submandibular bleeding in an EDTA-coated tube and analyzed for CAR T cell detection and expansion. In brief, the volume of blood was determined to calculate absolute values. Samples were then centrifuged and serum was collected. Cell pellets were resuspended in 500–1,000 µl of ACK lysis buffer (150 mM NH_4Cl, 10 mM $KHCO_3$ and 0.1 mM EDTA) for 1 min. Cells were then washed twice in fluorescence-activated cell sorting (FACS) buffer (PBS + 1% BSA). Samples were then stained with anti-CD45–PacificBlue (1:50, Biolegend), anti-CD4–PE/Dazzle594 (1:50, Biolegend), anti-CD8–FITC (1:50, Biolegend), anti-CCR7–AlexaFluor700 (1:50, Biolegend), anti-CD62L–PE (1:50, Biolegend), anti-CD45RO–PerCP/Cy5.5 (1:50, Biolegend), anti-CD45RA–APC/Fire750 (1:50, Biolegend), anti-programmed cell death protein 1 (PD1)–BV605 (1:50, Biolegend), anti-human leukocyte antigen (HLA)-DR–PE/Cy7 (1:50, Biolegend), anti-CD69–BV421 (1:50, Biolegend) and recombinant BCMA–AlexaFluor647 (10 nM, made in-house). Samples were run on an SP6800 Spectral Analyzer (Sony, FCS express software) or Aurora (Cytek, SpectroFlo). The flow rate and acquisition time were noted to calculate absolute values. The gating strategy was established and data were analyzed using FlowJo (Supplementary Fig. 20). All experiments were performed in a randomized fashion and included proper control groups. Animals were euthanized at the end of the experiment or when they met prespecified endpoints according to the IACUC protocols. Upon endpoint, major immune organs (spleen and bone marrow), as well as essential organs where possible metastatic lesions can form (that is, liver), were isolated, weighed and analyzed. In brief, the spleen was crushed using a plunger and passed through a 40-µm strainer to acquire a single-cell suspension. The bone marrow was aspirated using a 30-gauge insulin needle. The liver, lung and kidney were diced using surgical scissors in 3 ml of digestion buffer (1 ml of RPMI + 2 ml of PBS). Type 1 collagenase (Worthington) was added at a final concentration of 100 µg ml^{-1} and incubated at 37 °C for 1 h. The resulting samples were passed through a 40-µm strainer to acquire a single-cell suspension. Samples were then stained with the same antibodies used to stain blood samples and analyzed. The flow rate and acquisition time were noted to calculate absolute values.

Generation of the proteins

All genes were codon-optimized for HEK293 mammalian expression, synthesized and inserted into a vector expression system with a signal sequence. To facilitate production of the products, we generated stable HEK293T cell lines. Accordingly, HEK293T cells were transfected with pPAX2, pVSVG (packaging vectors) and the lentivirus plasmid containing the sequence of interest. The virus was harvested at 48, 72 and 96 h, sedimented at 20,000*g* for 2 h and resuspended in optiMEM medium. A new batch of HEK293T cells was then subjected to three rounds of transduction with the virus. Cells were allowed to recover in complete DMEM and were subjected to puromycin selection to retain only those cells that integrated the lentivirus plasmid. Cells were then expanded, washed with PBS and incubated in serum-free DMEM for 48–72 h. The supernatant was harvested and protein expression was confirmed by SDS–PAGE and immunoblotting. Proteins were then purified by adsorption onto a Ni-NTA metal affinity column. Nonspecifically bound proteins were removed by washing with a low concentration of imidazole (20 mM). The imidazole concentration was then increased to 250 mM, allowing recovery of the protein of interest. The protein was then further purified by size-exclusion chromatography and stored in 50 mM HEPES buffer (pH 7.5) at −80 °C until use.

Production of CAR T cells

For the BCMA CAR T cells, we used the anti-human BCMA scFv followed by the human 4-1BB and CD3ζ intracellular signaling domain[39]. The human signaling CAR construct was transduced into HEK293T cells that stably produce gammaretrovirus pseudotyped with the envelope of the feline endogenous virus (RD114)[40]. High viral titer clones were isolated using limiting dilution. The high expression clone was then seeded and grown in complete DMEM containing 10% FBS until 80% confluency. The medium was then exchanged with complete RPMI medium containing 10% FBS. After 24 h, the virus-containing medium was harvested, sterile-filtered using a 0.45-µm polyethersulfane filter and used for producing CAR T cells.

The production of CAR T cells was adapted from previous studies[41]. In brief, PBMCs were isolated from whole blood obtained from apheresis leukoreduction collars of platelet healthy donors using Ficoll gradient. Whole PBMCs were used. PBMCs were resuspended in RPMI medium containing 10% FBS, 200 IU per ml IL-2 (Teceleukin, BRB Preclinical Biologics Repository), 60 ng ml^{-1} IL-7 (glycosylated, BRB Preclinical Biologics Repository), 10 ng ml^{-1} IL-15 (BRB Preclinical Biologics Repository), 2 µg ml^{-1} anti-human CD3 (BRB Preclinical Biologics Repository) and 0.5 µg ml^{-1} anti-human CD28 (CD28.1 clone, Biolegend) at a cell concentration of 4×10^6 cells per ml in 3 ml of medium for every well of a six-well plate. After 24 h, cells were harvested, spun down and resuspended in 1 ml of fresh RPMI medium with FBS, IL-2, IL-15 and IL-7, in addition to 2 ml of medium harvested from anti-human BCMA CAR gammaretrovirus-producing cells. The PBMCs inoculated with gammaretrovirus were then plated onto retronectin-coated six-well plates (coated with 1 ml of 20 µg ml^{-1} retronectin in PBS for 24 h at 4 °C) at a concentration of 4×10^6 cells per ml in 3 ml for every well of a six-well non-tissue culture-treated plate. The cells underwent spinoculation in a centrifuge for 1 h at 2,000*g* at 30 °C. Afterward, cells were incubated at 37 °C. The transduction step was repeated once more with fresh

gammaretrovirus-containing medium, cytokines and spinoculation. Flow cytometry analysis was used to assess the transduction efficiency of the CAR transgene using the dsRed reporter gene and recombinant BCMA labeled with AlexaFluor647.

Flow cytometry analysis

FlowJo software was used for FlowSOM and fast interpolation (Fl)-based *t*-stochastic neighborhood embedding (tSNE) analyses. For FltSNE and FlowSOM analyses, CAR T cells from the spleen and bone marrow were downsampled and concatenated such that there was an equivalent number of cells between the analyzed conditions. For FltSNE, the maximum number of iterations was set to 1,000, perplexity was set to 20, θ was set to 0.5 and learning rate was set to 200.

Binding assays

Cells were washed once with FACS buffer (PBS + 1% BSA). They were then stained with various concentrations of the proteins and incubated on ice for 20 min. Cells were then washed twice with FACS buffer and stained with anti-FLAG AlexaFluor647 (1:500, Biolegend) on ice for 20 min. PBMCs were further stained with anti-CD3–FITC (1:100, Biolegend), anti-CD20–PE/Cy7 (1:100, Biolegend) and anti-CD11b–PacificBlue (1:100, Biolegend) on ice for 20 min. Cells were then washed twice with FACS buffer and analyzed using the BD FACSCanto II (Becton Dickinson). Flow cytometry data were analyzed using FlowJo software (Becton Dickinson).

pSTAT5 assay

Initially, CAR T cells were incubated in complete RPMI medium without the presence of cytokines (rested) for 24 h. Cells were then stained with CellTrace Blue (Invitrogen) or CellTracker Red (Invitrogen) for 30 min at 37 °C for the indicated conditions. Cells were washed once with complete RPMI + 10% FBS medium. CAR T cells stained with CellTracker Red were blocked using recombinant BCMA–CH3 (100 nM) for 20 min on ice while cells stained with CellTrace Blue were not blocked. Cells were then washed once with complete RPMI + 10% FBS medium followed by seeding of approximately 2×10^5 cells (the two separately stained cells cocultured or separately cultured) per well of a 96-well plate in the presence of serial dilutions of treatments or cytokine controls at 37 °C. After 5 min of incubation, cells were immediately fixed with 1.5% formaldehyde in PBS for 10 min at room temperature. Cells were then permeabilized with ice-cold 100% methanol for 20 min on ice. Fixed and permeabilized cells were washed twice with FACS buffer and then incubated with anti-STAT5 pY694–PE/Cy7 (1:200, Biolegend) for 30 min on ice. Cells were then washed twice with FACS buffer and analyzed using the BD FACSCanto II (Becton Dickinson). Flow cytometry data were analyzed using FlowJo (Becton Dickinson), dose–response curves were fitted to a logistic sigmoidal model and EC_{50} values and 95% confidence intervals (CIs) were calculated using Prism data analysis software (GraphPad).

Activation assay

Initially, CAR or nontransduced T cells were incubated in complete RPMI medium without the presence of cytokines (rested) for 24 h. Approximately 2×10^5 cells per well of a 96-well plate were then seeded in the presence of serial dilutions of treatments or cytokine controls at 37 °C for 24 h. Cells were then washed twice with FACS buffer. Primary staining was conducted with BCMA–CH3 for 20 min on ice to stain all CAR-expressing cells. Cells were washed with FACS buffer and stained with anti-CD69–BV421 (1:100, Biolegend) and anti-FLAG tag–AlexaFluor647 (1:500, Biolegend) for 20 min on ice. Cells were then washed twice with FACS buffer and analyzed using the BD FACSCanto II (Becton Dickinson). Flow cytometry data were analyzed using FlowJo (Becton Dickinson), dose–response curves were fitted to a logistic sigmoidal model and EC_{50} values and 95% CIs were calculated using Prism data analysis software (GraphPad).

CAR T cell killing assays

OPM2 cells, expressing GFP, were seeded at a concentration of approximately 1×10^5 cells per well of a 96-well flat-bottom plate. Either BCMA CAR T cells or nontransduced T cells were seeded at a concentration of approximately 1 or 2×10^5 CAR^+ cells per well (E:T ratio = 1:1 or 2:1) in the presence of serial dilutions of treatments or controls at 37 °C. Cells were then assessed for GFP-positive tumor cells using BD FACSCanto II (Becton Dickinson) 24, 48 and 72 h later and absolute numbers of live tumor cells were calculated. Dose–response killing curves were generated using Prism data analysis software (GraphPad).

Pharmacokinetic study

NSG mice were administered a dose of 8 mg kg^{-1} of BCMA–mutIL-2 by i.p. injection. Blood samples were collected from mice at various time points through intravenous tail-vein blood draw. After a 30-min period at room temperature, serum was isolated from the blood samples using centrifugation. Collected serum was analyzed using a sandwich ELISA detection assay. In brief, ELISA plates were coated with 5 µg ml^{-1} solution of purified anti-6xHis-tag antibody (Biolegend) overnight at 4 °C. The plate was washed with PBS and incubated with blocking buffer (PBS + 2% BSA) for 1 h at room temperature. The serum was diluted 1:50 and incubated for 2 h at room temperature. The plate was then washed with washing buffer (PBS + 0.05% Tween-20) and incubated with horseradish peroxidase-conjugated anti-FLAG tag antibody (Biolegend, 1:2500) for 1 h at room temperature. The plate was washed with washing buffer and incubated with TMB solution (Biolegend) for 20 min. The reaction was stopped using 2 N H_2SO_4 solution and absorbance was read using a spectrophotometer at 450 nm.

Cytokine detection assay

Serum collected from mice at different time points was first diluted 1:25. Two different methods were used to assess cytokine levels in the serum. The first method we used was an IFNγ ELISA kit (Biolegend). In brief, a 96-well plate was coated with IFNγ capture antibody overnight at 4 °C. The plate was washed with PBS-T (PBS + 0.1% Tween-20) and blocked with blocking buffer (PBS + 4% BSA) for 1 h at room temperature. The plate was then washed and incubated with diluted serum for 2 h at room temperature. Next, the plate was washed and incubated with biotinylated IFNγ detection antibody for 1 h at room temperature and then washed and incubated with avidin–horseradish peroxidase for 30 min at room temperature. TMB substrate was used as a detection reagent and 2 N H_2SO_4 was used as a stopping reagent. IFNγ levels were assessed by absorbance at 450 nm using a Luminometer. The second method we used was a flow cytometry-based immunoassay (Biolegend). In brief, our diluted serum was mixed with a precoated premixed bead slurry containing beads of different sizes and APC florescence, each conjugated to a different capture antibody. The bead–serum mixture was incubated for 2 h at room temperature. Upon washing the beads, the biotinylated detection antibodies were incubated for 2 h at room temperature followed by an additional 30 min at room temperature upon the addition of avidin–PE. The beads were analyzed by flow cytometry and differentiated by size and APC florescence, while the level of cytokines was assessed by PE florescence.

Preparing samples for scRNAseq

After animals were euthanized, cells derived from their bone marrow and spleen were isolated and converted into a single-cell suspension. Cells were counted and stained with AlexaFluor647-labeled BCMA, propidium iodide (PI) and 2 µl (1 µg) of Biolegend TotalSeq-C hashing antibody per 1 million cells in 100 µl of FACS wash buffer (2% FBS in PBS). Unique hashing antibodies were used for cells derived from the bone marrow and spleen of the BCMA–mutIL-2-treated and VHH–mutIL-2-treated mice. CAR T cells were sorted into PBS with 0.1% BSA and live cells were processed directly for droplet-based 5′-end parallel

scRNAseq. A total of 5,000 CAR T cells from the bone marrow and spleen of the BCMA–mutIL-2-treated mouse and 2,500 CAR T cells from the bone marrow and spleen of the VHH–mutIL-2-treated mouse (as more cells could not be obtained from the VHH–mutIL-2-treated mouse) were loaded onto the 10x channel with a recovery of 5,369 cells. The 10x Genomics chromium single-cell 5′ library and gel bead kit v2 were used according to the manufacturer's protocol (10x Genomics). scRNAseq libraries were sequenced through Novogene on the NovaSeq PE150 at a sequencing depth of 20,000 reads per cell for the 5′ gene expression library and at a sequencing depth of 5,000 reads per cell for the V(D)J and cell surface protein libraries.

scRNAseq analysis

Gene counts for each sample were obtained using the CellRanger multifunction through 10x cloud computing and pooled using the CellRanger aggr function to produce a .h5 file that could be loaded into R as a Seurat object. The Seurat pipeline was applied for quality control filtering (number of total counts, <20,000; number of molecular identifiers, <6,000; ribosomal RNA, <10% of the reads). Data were then scaled and normalized using scTransform and original samples were traced back using the demultiplexing function HTODemux(). The phenotype of the cells was then determined using projection of our sample to the Seurat pbmc_multimodal dataset using the FindTransferAnchors() and FindQuery() workflow. The FindMarkers() function was used to find differentially expressed genes between chosen groups. The heat maps were generated with the DoHeatmap() function with a downsampling of 500 cells. Gene Scores were obtained by creating a list of the genes of interest, which was given as the feature for the function AddModuleScore().

Preparing samples for bulk RNAseq

CAR T cells were incubated in complete RPMI medium without the presence of cytokines for 24 h. A 96-well plate was seeded with approximately 2×10^5 cells per well in the presence of 10 nM treatment or controls at 37 °C for 2 h. Cells were washed with FACS buffer and left at 37 °C for 2 or 22 h (4-h and 24-h time points). Cells were stained with anti-CD8–FITC (1:50, Biolegend), anti-CD4–PE/Dazzle594 (1:50, Biolegend) and AlexaFluor647-labeled BCMA and sorted on the Sony Sorter MA900. In total, 10,000 $CD4^+$ and 10,000 $CD8^+$ cells were sorted per condition. The SMART-seq mRNA library preparation kit (Takara Bio) was used to generate mRNA libraries, with each replicate tagged with a unique index. Libraries were pooled and sequenced through Novogene at a sequencing depth of 20 million reads per sample.

Bulk RNAseq

Gene counts for the samples were obtained by trimming the FASTQ files and transcript quantification using the RNAlysis software. Gene names were obtained from the *Homo sapiens* Ensembl database with biomaRt and differential expression between different conditions was determined using the DESeq2 pipeline. Volcano plots were drawn using the EnhancedVolcano library (https://github.com/kevinblighe/EnhancedVolcano), with cutoffs at log(FC) > |2| and P value > 10^{-6}. Heat maps were generated using the pheatmap library. Gene set enrichment analysis was performed using the pipeline of the fgsea package with the ranking metric being $-\log_{10}(P \text{ value}) \times \text{sign}$ (fold change) and basing the computations on the hallmark pathways of the MSigDB collection.

Microscopy imaging

For the microscopy imaging experiments, BCMA CAR T cells with a transduction efficiency of ~50%, as determined by flow cytometry, were used. First, the cells were allowed to rest for 1 day in a complete RPMI solution without cytokines. The rested cells were initially stained with 10 µM of CellTracker Blue CMAC (Invitrogen, C2110) solution in complete RPMI medium for 30 min at 37 °C. For the experiment shown in Supplementary Fig. 3, 300,000 cells were seeded onto precoated poly(D-lysine) glass coverslips (Neuvitro GG-12-1.5-PDL) and incubated at 37 °C for 45 min to adhere to the coverslips. The CAR T cells were subsequently incubated with the indicated treatments (2 nM AlexaFluor647-labeled BCMA–mutIL-2, BCMA–CH3 or VHH–mutIL-2 or no treatment) in complete RPMI medium under specified conditions. AlexaFluor647-labeled proteins were made using a sortase reaction, as previously reported[42]. The samples were then washed two times with PBS + 2% BSA solution, then fixed using Cytofix buffer (BD, 554655) and mounted using Antifade mounting solution. Finally, the slides were imaged using an inverted bright-field microscope (Leica Thunder Imager, Leica LAS X software) equipped with a ×63 objective. The imaging process involved the use of the bright-field channel, as well as three distinct fluorescent channels: CellTracker Blue, dsRed and AlexaFluor647. High-resolution 16-bit images were acquired with a pixel size of 0.1026 µm. For the experiment shown in Supplementary Fig. 4, 200,000 cells labeled with CellTracker Blue were mixed with the indicated treatments (AlexaFluor647-labeled BCMA–mutIL-2 or BCMA–CH3; 2 nM) and subsequently seeded into a µ-Slide eight-well glass-bottom plate (Ibidi, catalog number 80807). Live imaging was conducted using a CSU-W1 SoRa confocal microscope equipped with a ×60 objective, maintaining constant laser settings, temperature (37 °C) and CO_2 levels (5%) throughout the imaging period. High-resolution 16-bit images were acquired with a pixel size of 0.108 µm at the indicated time points.

Image processing

For Supplementary Fig. 3, the acquired images were subjected to analysis using ImageJ software. Initially, the CellTracker Blue channel was used to segment and delineate the cellular cytoplasm and membrane. This channel was converted into a binary image using the Huang method for thresholding. Subsequently, cells were identified through the application of the 'analyze particles' function, wherein particles with a size greater than five pixels and a circularity exceeding 0.05 were selected. This process generated region of interest (ROI) areas. Following the identification of ROIs, the ROI for each cell was scaled by factors ranging from 0.1 to 2.0, while maintaining the same centroid. ROIs with scaling factors of 0.8 and 1.4 were designated as representing the cytoplasm and the entire cell, respectively. The area between these two ROIs was defined as the membrane region. Finally, the mean and integrated intensities of the other channels were measured within the predetermined ROIs after background subtraction. For Supplementary Fig. 4, binarized fluorescent images from the AlexaFluor647 and CellTracker Blue channels were used for analysis; cell masks generated from the binary of the CellTracker Blue channel were eroded into ten concentric rings. Relative intensity, defined as the number of pixels within a ring positive for AlexaFluor647 fluorescence divided by the total number of pixels within a ring, was normalized by the area under the curve. To quantify the degree of internalization, a moment of internalization was defined as $M = C\sum_{0.1}^{1} n^2 \times I(n)$, where the normalized relative intensity I within each concentric ring is weighted by its distance n toward the cell exterior from center.

Reporting summary

Further information on research design is available in the Nature Portfolio Reporting Summary linked to this article.

Data availability

All relevant data are provided in this paper and Supplementary Information. RNAseq data generated in this study are available from the National Center for Biotechnology Information Sequence Read Archive (PRJNA1118916). The Ensembl *H. sapiens* database (https://useast.ensembl.org/Homo_sapiens/Info/Index) was used to identify RNA transcripts. Any remaining raw data are available from the corresponding author upon reasonable request.

Code availability

No custom code was developed for the analyses of the results.

References

38. Smith, E. L. et al. Development and evaluation of an optimal human single-chain variable fragment-derived BCMA-targeted CAR T cell vector. *Mol. Ther.* **26**, 1447–1456 (2018).
39. Works, M. et al. Anti-B-cell maturation antigen chimeric antigen receptor T cell function against multiple myeloma is enhanced in the presence of lenalidomide. *Mol. Cancer Ther.* **18**, 2246–2257 (2019).
40. Ward, M. et al. A stable murine-based RD114 retroviral packaging line efficiently transduces human hematopoietic cells. *Mol. Ther.* **8**, 804–812 (2003).
41. Li, G., Park, K. & Davila, M. L. Gammaretroviral production and T cell transduction to genetically retarget primary T cells against cancer. *Methods Mol. Biol.* **1514**, 111–118 (2017).
42. Guimaraes, C. P. et al. Site-specific C-terminal and internal loop labeling of proteins using sortase-mediated reactions. *Nat. Protoc.* **8**, 1787–1799 (2013).

Acknowledgements

Funding was provided by the Dana-Farber Cancer Institute Innovation Research Fund Award (M.R.), the Parker Institute for Cancer Immunotherapy (M.R., Grant no. C-03160), a Blavatnik Therapeutics Challenge Award (M.R., Grant no. 223813.5124476.0008) and an American Cancer Society postdoctoral fellowship (T.R., Grant no. PF-20-015-01-CCE). We thank the Boston University Micro and Nano Imaging Core Facility and Photonics Center for providing optical imaging support through Natural Science Foundation Major Research Instrumentation Awards 2215990 and DP2HL168562 (H.T.N.). We are grateful to I. Rubin-Bejerano, M. Namchuk, E. Smith and M. Goudarzi for helpful discussions. We thank Louise Clark for her technical assistance. We thank the National Cancer Institute-sponsored Biological Resource Branch Preclinical Biologics Repository for providing the anti-CD3 antibody (OK3) and IL-2, IL-7 and IL-15. We extend our gratitude to the microscopy core and the flow cytometry core within the Department of Cancer Immunology, as well as the dedicated animal facility staff at the Dana-Farber Cancer Institute and the Boston Children's Hospital, for their invaluable support throughout this project.

Author contributions

T.R., S.R.M., H.M., B.B.V.L., A.S.F., L.M., K.R., R.K., A.W., Z.F., M.C., A.K., A.N., U.-J.L., H.H.A., L.B., E.S., S.C.U., J.B., S.T., J.E.R., E.C., H.S. and J.P. designed and performed experiments and analyzed the results. C.A.J., O.N., H.T.N. and K.W.W. provided specific experimental advice and technical support. M.R. planned the experiments, analyzed the data and wrote the paper with help from the other authors.

Competing interests

T.R. and M.R. are inventors on a related patent application. M.R. is the scientific founder of Koi Biotherapeutics. C.A.J. serves as a consultant for Kite/Gilead, Novartis, BMS, Sana, Synthekine, Janssen, Miltenyi, Caribou, Galapagos, ADC Therapeutics, AstraZeneca and Abbvie, and receives research funding from Kite/Gilead. O.N. receives research support from Takeda and Janssen, participates on advisory boards for Bristol Myers Squibb, Janssen, Sanofi, Takeda and GPCR Therapeutics, and receives honoraria from Pfizer. The other authors declare no competing interests.

Additional information

Supplementary information The online version contains supplementary material available at https://doi.org/10.1038/s41587-024-02339-4.

Correspondence and requests for materials should be addressed to Mohammad Rashidian.

Peer review information *Nature Biotechnology* thanks Christina Amatya and the other, anonymous, reviewer(s) for their contribution to the peer review of this work.

nature portfolio

Corresponding author(s): Mohammad Rashidian

Last updated by author(s): Feb 7, 2024

Reporting Summary

Nature Portfolio wishes to improve the reproducibility of the work that we publish. This form provides structure for consistency and transparency in reporting. For further information on Nature Portfolio policies, see our Editorial Policies and the Editorial Policy Checklist.

Statistics

For all statistical analyses, confirm that the following items are present in the figure legend, table legend, main text, or Methods section.

n/a	Confirmed
☐	☒ The exact sample size (*n*) for each experimental group/condition, given as a discrete number and unit of measurement
☐	☒ A statement on whether measurements were taken from distinct samples or whether the same sample was measured repeatedly
☐	☒ The statistical test(s) used AND whether they are one- or two-sided *Only common tests should be described solely by name; describe more complex techniques in the Methods section.*
☐	☒ A description of all covariates tested
☐	☒ A description of any assumptions or corrections, such as tests of normality and adjustment for multiple comparisons
☐	☒ A full description of the statistical parameters including central tendency (e.g. means) or other basic estimates (e.g. regression coefficient) AND variation (e.g. standard deviation) or associated estimates of uncertainty (e.g. confidence intervals)
☐	☒ For null hypothesis testing, the test statistic (e.g. *F*, *t*, *r*) with confidence intervals, effect sizes, degrees of freedom and *P* value noted *Give P values as exact values whenever suitable.*
☒	☐ For Bayesian analysis, information on the choice of priors and Markov chain Monte Carlo settings
☒	☐ For hierarchical and complex designs, identification of the appropriate level for tests and full reporting of outcomes
☒	☐ Estimates of effect sizes (e.g. Cohen's *d*, Pearson's *r*), indicating how they were calculated

Our web collection on statistics for biologists contains articles on many of the points above.

Software and code

Policy information about availability of computer code

Data collection	BD FACSDiva v6.1.3, Sony Spectral Analyzer FCS express software, and Cytek SpectroFlo v3.1 was used to obtain flow cytometry data. Leica LAS X v1.4.6 software was used to obtain microscopy data. Single cell RNA sequencing data was obtained using Illumina NovaSeq X-plus.
Data analysis	Flow cytometry data was analyzed using BD FlowJo v10.10.0. ImageJ v1.54i and Python 3.12.3 were used to analyze and quantify microscopy data. Single cell RNA sequencing data was first processed and curated using the 10x Genomics cloud analysis. Further downstream analysis was conducted using Seurat v4.3.0, an R package designed for QC, analysis, and exploration of single cell RNA sequencing data. Bulk RNAseq was processed and quantified using RNAlysis v3.12.0.

For manuscripts utilizing custom algorithms or software that are central to the research but not yet described in published literature, software must be made available to editors and reviewers. We strongly encourage code deposition in a community repository (e.g. GitHub). See the Nature Portfolio guidelines for submitting code & software for further information.

Data

Policy information about availability of data

All manuscripts must include a data availability statement. This statement should provide the following information, where applicable:

- Accession codes, unique identifiers, or web links for publicly available datasets
- A description of any restrictions on data availability
- For clinical datasets or third party data, please ensure that the statement adheres to our policy

All relevant data are provided in this paper and Supplementary Information. RNA sequencing data generated in this study are available at the NCBI Sequence Read Archive (PRJNA1118916). The Ensembl homo sapien database (https://useast.ensembl.org/Homo_sapiens/Info/Index) was used to identify RNA transcripts. Any remaining raw data will be available from the corresponding author upon reasonable request.

Human research participants

Policy information about studies involving human research participants and Sex and Gender in Research.

Reporting on sex and gender	No human research was conducted.
Population characteristics	No human research was conducted.
Recruitment	No human research was conducted.
Ethics oversight	No human research was conducted.

Note that full information on the approval of the study protocol must also be provided in the manuscript.

Field-specific reporting

Please select the one below that is the best fit for your research. If you are not sure, read the appropriate sections before making your selection.

☒ Life sciences ☐ Behavioural & social sciences ☐ Ecological, evolutionary & environmental sciences

For a reference copy of the document with all sections, see nature.com/documents/nr-reporting-summary-flat.pdf

Life sciences study design

All studies must disclose on these points even when the disclosure is negative.

Sample size	For in vivo mouse experiments, we utilized 4-6 mice per treatment group in order to reproducibly observe statistically significant differences. Sample size was not pre-determined due to material limitations of mice (availability, etc.). For in vitro studies, all studies were done according to sample availability. No sample size calculations were performed.
Data exclusions	Data from tissue culture analysis was only excluded if contaminated.
Replication	All in vitro experiments were performed independently. Replicates of each individual experiment is stated in the figure legend. Experimental findings were reproduced with similar results. All in vivo mice experiments were performed independently and were conducted with sufficient numbers of mice to ensure reproducibility.
Randomization	We conducted stratified random sampling to assign mice to experimental or control groups. For tissue culture experiments we randomly placed treatment and control groups on assay plates
Blinding	Experiments were not performed in a blinded fashion. All data was batch analyzed by software in a parallel manner with relevant positive and negative controls.

Reporting for specific materials, systems and methods

We require information from authors about some types of materials, experimental systems and methods used in many studies. Here, indicate whether each material, system or method listed is relevant to your study. If you are not sure if a list item applies to your research, read the appropriate section before selecting a response.

Materials & experimental systems

n/a	Involved in the study
☐	☒ Antibodies
☐	☒ Eukaryotic cell lines
☒	☐ Palaeontology and archaeology
☐	☒ Animals and other organisms
☒	☐ Clinical data
☒	☐ Dual use research of concern

Methods

n/a	Involved in the study
☒	☐ ChIP-seq
☐	☒ Flow cytometry
☒	☐ MRI-based neuroimaging

Antibodies

Antibodies used

anti-CD45-PacificBlue (1:50, Biolegend, Cat#304022), anti-CD4-PE/Dazzle594 (1:50, Biolegend, Cat#317448), anti-CD8-FITC (1:50, Biolegend, Cat#344704), anti-CCR7-AlexaFluor700 (1:50, Biolegend, Cat#353244), anti-CD62L-PE (1:50, Biolegend, Cat#304806), anti-CD45RO-PerCP/Cy5.5 (1:50, Biolegend, Cat#304222), anti-CD45RA-APC/Fire750 (1:50, Biolegend, Cat#304152), anti-PD1-BV605 (1:50, Biolegend, Cat#329924), anti-HLA-DR-PE/Cy7 (1:50, Biolegend, Cat#307616), anti-CD69-BV421 (1:50, Biolegend, Cat#310930), recombinant BCMA-AlexaFlour647 (10nM, made in-house), anti-human CD3 (1:500, Cat# OKT3, BRB Preclinical Biologics Repository), and anti-human CD28 (1:1000, CD28.1 clone, Biolegend, Cat#302902), anti-DYKDDDDK Epitope Tag-AlexaFlour647 (1:500, anti-FLAG tag, Biolegend, Cat#637316), anti-CD3-FITC (1:100, Biolegend, Cat#317306), anti-CD20-PE/Cy7 (1:100, Biolegend, Cat#302312), anti-CD11b-PacificBlue (1:100, Biolegend, Cat#301315), anti-STAT5 pY694-PE/Cy7 (1:200, Biolegend, Cat#936908), anti-6-His Epitope Tag Antibody (5mg/mL, Biolegend, Cat#906102)

Validation

All antibodies were validated according to the manufacturer's statement. Validation data is available on vendors website. All antibodies purchased in this study have valid citations. In-house antibodies were validated using established cell lines expressing the target. Dose response curves were generated and EC50 was quantified. Appropriate negative controls were used to established specificity.

Eukaryotic cell lines

Policy information about cell lines and Sex and Gender in Research

Cell line source(s)

OPM2 (DSMZ, #ACC 50)
HEK293T (ATCC #CRL-3216)
Human Peripheral Blood Mononuclear Cells (PBMC) (Commercial sources (Charles River Laboratories, and Crimson Core BWH)

Authentication

HEK293T cells were authenticated using short tandem repeat (STR) markers from ATCC. OPM2 and donor PBMC samples were not authenticated. OPM2 cells were confirmed to express BCMA.

Mycoplasma contamination

All cells were tested and negative for Mycoplasma.

Commonly misidentified lines
(See ICLAC register)

No commonly misidentified cell line was used.

Animals and other research organisms

Policy information about studies involving animals; ARRIVE guidelines recommended for reporting animal research, and Sex and Gender in Research

Laboratory animals

Mus Musculus: NOD-scid IL2Rgnull (NSG, Jackson Lab Strain#005557) and NOD-scid H2-K1null H2-Ab1null H2-D1null IL2Rgnull (NSG-MHC I/II double knockout [DKO], Jackson Lab Strain#025216), 5-8 week mice, both male and female used in our studies. All mice were housed at Dana Farber Cancer Institute (DFCI) or Boston Children's Hospital (BCH) under the following housing conditions: temperatures between 70-74F, humidity between 30% to 70%, a light cycle ON at 6:00 AM and OFF at 6:00 PM, with a negative pressure room.

Wild animals

No wild animals were used in this study

Reporting on sex

Each experiment pertaining to mice utilized both sexes. Sex was taken into account when assigning mice into groups in order to have sex-matched controls and experimental cohorts.

Field-collected samples

No field collected samples were used in this study

Ethics oversight

All experiments adhered to the pertinent ethical and safety protocols. The studies were carried out under the oversight of the Dana-Farber Cancer Institute Institutional Animal Care and Use Committee (protocol no. 20-006), and the Boston Children's Hospital Committee on Animal Care (protocol number BCH 00001455).

Note that full information on the approval of the study protocol must also be provided in the manuscript.

Flow Cytometry

Plots

Confirm that:

☒ The axis labels state the marker and fluorochrome used (e.g. CD4-FITC).

☒ The axis scales are clearly visible. Include numbers along axes only for bottom left plot of group (a 'group' is an analysis of identical markers).

☒ All plots are contour plots with outliers or pseudocolor plots.

☒ A numerical value for number of cells or percentage (with statistics) is provided.

Methodology

Sample preparation	Cells were either harvested from tissue culture or from mice blood, spleen, bone marrow, liver, lung, and kidney. Peripheral blood from mice were obtained by submandibular bleeding in an EDTA-coated tube and analyzed for CAR T cell detection and expansion. Samples were then centrifuged, and serum separated from cells. Upon endpoint mice were sacrificed and spleen, bone marrow, liver, lung, and kidney were harvested. Spleen was crushed using a plunger. Bone marrow was aspirated using a 30-gauge insulin needle. Liver, lung, and kidney were diced using surgical scissors in 3 mL of Digestion buffer (1mL RPMI + 2mL PBS). Collagenase, Type 1 (Worthington) was added at a final concentration of 100 ug/mL and incubated at 37°C for 1 hour. The resulting samples were passed through a 40 µm strainer to acquire a single-cell suspension. Harvested cells were centrifuged and pellets were resuspended in 500-1000 uL of ACK Lysis Buffer (150 mM NH4Cl, 10mM KHCO3, 0.1 mM EDTA) for 1 minute to lyse RBCs. Cells were then washed twice in FACS buffer, PBS + 1% Bovine Serum Albumin (BSA), and stained with appropriate antibodies at 4°C. Cells were then washed twice, resuspended in FACS buffer, and analyzed.
Instrument	BD FACSCanto II, Sony SP6800 Spectral Analyzer, and Cytek Aurora
Software	Software used to collect data was BD FACS Diva, Sony FCS Express, or Cytek SpectroFlo. BD FlowJo v10.10.0 was used to analyze flow cytometry data.
Cell population abundance	Sony MA900 was used for sorting. The abundance of the population we would sort was between 40-80% of the cell population.
Gating strategy	Preliminary FSC/SSC gating of the starting cell population was determined using backgating of positive controls. Boundaries of negative population is determined using either unstained samples or staining of a negative population.

☒ Tick this box to confirm that a figure exemplifying the gating strategy is provided in the Supplementary Information.